

1 Anti-clustering in the national SARS-CoV-2 2 daily infection counts

3 Boudewijn F. Roukema^{1,2}

4 ¹Institute of Astronomy, Faculty of Physics, Astronomy and Informatics, Nicolaus
5 Copernicus University, Grudziadzka 5, 87-100 Toruń, Poland

6 ²Univ Lyon, Ens de Lyon, Univ Lyon1, CNRS, Centre de Recherche Astrophysique de
7 Lyon UMR5574, F-69007, Lyon, France

8 Corresponding author:
9 Boudewijn F. Roukema¹

10 Email address: boud@astro.uni.torun.pl

11
12 Cite as: *Roukema, B.F., 2021, PeerJ, 9:e11865 [arXiv:2007.11779]*

13
14 DOI: 10.7717/peerj.11856

15 source DOI: 10.5281/zenodo.5261231

16 ABSTRACT

17 The noise in daily infection counts of an epidemic should be super-Poissonian due to intrinsic epidemio-
18 logical and administrative clustering. Here, we use this clustering to classify the official national SARS-
19 CoV-2 daily infection counts and check for infection counts that are unusually anti-clustered. We adopt
20 a one-parameter model of ϕ_i' infections per cluster, dividing any daily count n_i into n_i/ϕ_i' 'clusters', for
21 'country' i . We assume that n_i/ϕ_i' on a given day j is drawn from a Poisson distribution whose mean
22 is robustly estimated from the 4 neighbouring days, and calculate the inferred Poisson probability P'_{ij} of
23 the observation. The P'_{ij} values should be uniformly distributed. We find the value ϕ_i that minimises
24 the Kolmogorov–Smirnov distance from a uniform distribution. We investigate the (ϕ_i, N_i) distribution,
25 for total infection count N_i . We consider consecutive count sequences above a threshold of 50 daily
26 infections. We find that most of the daily infection count sequences are inconsistent with a Poissonian
27 model. Most are found to be consistent with the ϕ_i model. The 28-, 14- and 7-day least noisy sequences
28 for several countries are best modelled as sub-Poissonian, suggesting a distinct epidemiological fam-
29 ily. The 28-day least noisy sequence of Algeria has a preferred model that is strongly sub-Poissonian,
30 with $\phi_i^{28} < 0.1$. Tajikistan, Turkey, Russia, Belarus, Albania, United Arab Emirates, and Nicaragua have
31 preferred models that are also sub-Poissonian, with $\phi_i^{28} < 0.5$. A statistically significant ($P^\tau < 0.05$) cor-
32 relation was found between the lack of media freedom in a country, as represented by a high *Reporters*
33 *sans frontières* Press Freedom Index (PFI²⁰²⁰), and the lack of statistical noise in the country's daily
34 counts. The ϕ_i model appears to be an effective detector of suspiciously low statistical noise in the
35 national SARS-CoV-2 daily infection counts.

36 1 INTRODUCTION

37 The daily counts of new, laboratory-confirmed infections with severe acute respiratory syndrome coro-
38 navirus 2 (SARS-CoV-2) constitute one of the key statistics followed by citizens and health agen-
39 cies around the world in the ongoing 2019–2020 coronavirus disease 2019 (COVID-19) pandemic
40 (Huang et al. 2020b; Li et al. 2020). Can these counts be classified in a way that makes as few epi-
41 demiological assumptions as possible, as motivation for deeper analysis to either validate or invalidate
42 the counts? While full epidemiological modelling and prediction is a vital component of COVID-19
43 research (Chowdhury et al. 2020; Kim et al. 2020; Molina-Cuevas 2020; Jiang, Zhao & Shao 2021;
44 Afshordi et al. 2020), these cannot be accurately used to study the pandemic as a whole – a global phe-
45 nomenon by definition – if the data at the global level is itself inaccurate. Knowledge of the global
46 state of the current pandemic is weakened if any of the national-level SARS-CoV-2 infection data have

47 been artificially interfered with by the health agencies providing that data or by other actors involved
48 in the chain of data lineage (Thomas et al., 2017). Since personal medical data are private information,
49 only a limited number of individuals at health agencies are expected to be able to check the validity
50 of these counts based on original records. Nevertheless, artificial interventions in the counts could
51 potentially reveal themselves in statistical properties of the counts. Unusual statistical properties in a
52 wide variety of quantitative data sometimes appear, for example, as anomalies related to Benford's law
53 (Newcomb 1881; Nigrini & Miller 2009), as in the 2009 first round of the Iranian presidential election
54 (Roukema, 2014, 2015; Mebane, 2010). Benford's law analysis has been used to argue that countries with
55 higher democracy indices, high gross domestic product, and better health system indices tend to have
56 a lower probability of having manipulated their key COVID-19 related cumulative counts (confirmed
57 cases and deaths, Balashov, Yan & Zhu 2021). For other Benford's law COVID-19 count analyses,
58 see Koch & Okamura (2020) and Lee et al. (2020). For a case-specific analysis of the lack of noise in
59 governmental medical data, see the analysis of official deceased-donor organ-donation data from China
60 (Robertson, Hinde & Lavee, 2019), using methods different to the one introduced in this article. For the
61 politics of organisational strategies regarding open government data, see Ruijter et al. (2019).

62 Here, we check the compatibility of noise in the official national SARS-CoV-2 daily infection counts,
63 $n_i(t)$, for country¹ i on date t , with expectations based on the Poisson distribution (Poisson (1837); for a
64 review, see, e.g., Johnson et al. 2005). The Poisson distribution is motivated by the one-day time scale for
65 an infection count being several times shorter than the dominant time scale involved, the incubation time
66 scale, estimated at about five days (Lauer et al., 2020; Yang et al., 2020), with a 95% confidence interval
67 (CI) from about one to 15 days (Yang et al., 2020). Since each infected person typically infects about two
68 to three others ($R_0 \sim 2.4\text{--}3.3$ at 95% (CI), Billah et al. 2020), these secondarily infected people would
69 typically be assessed as SARS-CoV-2 positive on independent days, if they were diagnosed immediately
70 after the onset of symptoms, with instantaneous laboratory testing and test results reported instantly in
71 the official national count data. In reality, delays for diagnosis, testing and reporting and collating the test
72 results are random processes which should further add delays that reduce correlations among positive
73 test results between distinct nearby days; a Poissonian process is a simple hypothesis for each of these
74 separate processes. Poisson processes are both additive and infinitely divisible (Johnson et al., 2005, §4),
75 so the combination of these processes can reasonably yield an overall Poisson process.

76 However, it is unlikely that any real count data will be fully modelled by a Poisson distribution, both
77 due to the complexity of the logical tree of time-dependent intrinsic epidemiological infection as well
78 as administrative effects in the SARS-CoV-2 testing procedures, and the sub-national and national level
79 procedures for collecting and validating data to produce a national health agency's official report. In
80 particular, clusters of infections on a scale of ϕ_i^t infections per cluster, either intrinsic or in the testing
81 and administrative pipeline, would tend to cause relative noise to increase from a fraction of $1/\sqrt{n_i}$
82 for pure Poisson noise up to $\sqrt{\phi_i^t/n_i}$, greater by a factor of $\sqrt{\phi_i^t}$. This overdispersion has been found,
83 for example, for SARS-CoV-2 transmission (Endo et al., 2020; He et al., 2020) and for COVID-19 death
84 rate counts in the United States (Kim et al., 2020).

85 In contrast, it is difficult to see how anti-Poissonian smoothing effects could occur, unless they were
86 imposed administratively. For example, an administrative office might impose (or have imposed on it by
87 political authorities) a constraint to validate a fixed or slowly and smoothly varying number of SARS-
88 CoV-2 test result files per day, independently of the number received or queued; this would constitute an
89 example of an artificial intervention in the counts that would weaken the epidemiological usefulness of
90 the data.

91 A one-parameter model to allow for the clustering is proposed in this paper, and used to classify the
92 counts. We allow the parameter to take on an effective anti-clustering value, in order to allow the data
93 to freely determine its optimal value, without forcing overdispersion. While a distribution of clustering
94 values for a given country is likely to be more realistic than a single value, Occam's razor favours
95 adding as few parameters as possible. For example, a power-law distribution of arbitrary (negative)
96 index would require a second parameter to truncate the tail in non-convergent cases. While the one-
97 parameter anti-clustering value is a simplified model, it has the advantage of allowing a straightforward,
98 though simplified, interpretation in terms of clustering. If the one-parameter method proposed here is

¹No position is taken in this paper regarding jurisdiction over territories; the term 'country' is intended here as a neutral term without supporting or opposing the formal notion of state. Apart from minor changes for technical reasons, the 'countries' are defined by the data sources.

99 found to viable, then the method could be extended by including models of directly observed estimates
100 of SARS-CoV-2 clustering.

101 As an alternative to this clustering model, we also consider a negative binomial distribution
102 (e.g. Johnson et al., 2005, §5). Lloyd-Smith et al. (2005) found the negative binomial distribution, as a
103 mix of Poisson distributions over a Gamma distribution, to be better at modelling secondary infections by
104 SARS-CoV-1 (and other infectious agents) than Poisson and geometric distributions, quantifying what
105 are referred to as ‘superspreader’ events in an epidemic. This has also been found to be relevant to
106 SARS-CoV-2 secondary infections (Endo et al., 2020; He et al., 2020). However, since the negative bi-
107 nomial model only allows overdispersion with respect to the Poisson model, it is unlikely to provide the
108 best model for data which may have been artificially modified to the extent of becoming sub-Poissonian.
109 More in-depth models of clustering, called ‘burstiness’ in stochastic models of discrete event counts,
110 include power-law models (Barabási, 2005; Goh & Barabasi, 2006).

111 The method is presented in §2. Section §2.1 describes the choice of data set and the definition,
112 for any given country, of a consecutive time sequence that has high enough daily infection counts for
113 Poisson distribution analysis to be reasonable. The method of analysis is given in §2.3 for full sequences
114 (§2.3.1), subsequences (§2.3.2) and alternatives to the main method (§2.4). Results are presented in §3.
115 A non-parametric comparison with the *Reporters sans frontières* Press Freedom Index, which should
116 not have any relation to noise in SARS-CoV-2 daily counts in the absence of a sociological connection,
117 is provided in §3.3. Qualitative discussion of the results is given in §4. Conclusions are summarised
118 in §5. This work is intended to be fully reproducible by independent researchers using the MANEAGE
119 framework; it was produced using commit e217f39 of the live GIT repository [https://codeberg.
120 org/boud/subpoisson](https://codeberg.org/boud/subpoisson) on a computer with Little Endian x86_64 architecture; the source is archived
121 at zenodo.5261231 and swh:1:rev:eb46500ec25b9584324656d4f3f730cb0fdeba7b.

122 2 METHOD

123 2.1 SARS-CoV-2 infection data

124 Two obvious choices of a dataset for national daily SARS-CoV-2 counts would be those provided by
125 the World Health Organization (WHO)² or those curated by the Wikipedia *WikiProject COVID-19 Case
126 Count Task Force*³ in *medical cases chart* templates (hereafter, C19CCTF). While WHO has published
127 a wide variety of documents related to the COVID-19 pandemic, it does not appear to have published
128 details of how national reports are communicated to it and collated. Given that most government agen-
129 cies and systems of government procedures tend to lack transparency, despite significant moves towards
130 forms of open government (Yu & Robinson, 2012) in many countries, data lineage tracing from national
131 governments to WHO is likely to be difficult in many cases. In contrast, the curation of official gov-
132 ernment SARS-CoV-2 daily counts by the Wikipedia *WikiProject COVID-19 Case Count Task Force*
133 follows a well-established technology of tracking data lineage. The Wikipedia community high-tempo
134 collaborative editing that has taken place in response to the COVID-19 pandemic is well quantified
135 (Keegan & Tan, 2020). The John Hopkins University Center for Systems Science and Engineering cu-
136 rated set of official COVID-19 data is discussed below.

137 Unfortunately, it is clear that in the WHO data, there are several cases where two days’ worth of
138 detected infections appear to be listed by WHO as a sequence of two days j and $j + 1$ on which all
139 the infections are allocated to the second of the two days, with zero infections on the first of the pair.
140 There are also some sequences in the WHO data where the day listed with zero infections is separated
141 by several days from a nearby day with double the usual amount of infections. This is very likely an
142 effect of difficulties in correctly managing world time zones, or time zone and sleep schedule effects, in
143 any of several levels of the chains of communication between health agencies and WHO. In other words,
144 there are several cases where a temporary sharp jump or drop in the counts appears in the data but is
145 reasonably interpreted as a timing artefact. Whatever the reason for the effect, this effect will tend to
146 confuse the epidemiological question of interest here: the aim is to globally characterise the noise and to
147 highlight countries where unusual smoothing may have taken place.

148 We quantify this jump/drop problem as follows. We consider a pair of days j , $j + 1$ for a given
149 country to be a jump if the absolute difference in counts, $|n_i(j + 1) - n_i(j)|$, is greater than the mean,

²[https://covid19.who.int/WHO-COVID-19-global-data.csv;\(archive\)](https://covid19.who.int/WHO-COVID-19-global-data.csv;(archive))

³[https://en.wikipedia.org/w/index.php?title=Wikipedia:WikiProject_COVID-19/
Case_Count_Task_Force&oldid=1001119689](https://en.wikipedia.org/w/index.php?title=Wikipedia:WikiProject_COVID-19/Case_Count_Task_Force&oldid=1001119689)

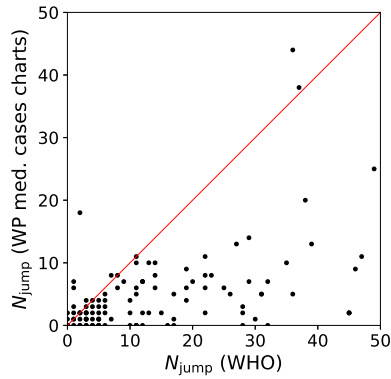


Figure 1. Number N_{jump} of sudden jumps or drops in counts on adjacent days in WHO and Wikipedia *WikiProject COVID-19 Case Count Task Force medical cases chart* national daily SARS-CoV-2 infection counts for countries present in both data sets. A line illustrates equal quality of the two data sets. The C19CCTF version of the data is clearly less affected by sudden jumps than the WHO data. Plain-text table: zenodo.5261231/WHO_vs_WP_jumps.dat.

150 $(n_i(j+1) + n_i(j))/2$. In the case of a pair in which one value is zero, the absolute difference is twice
 151 the mean, and the condition is necessarily satisfied. We evaluate the number of jumps N_{jump} for both the
 152 WHO data and the C19CCTF *medical cases chart* data, starting, for any given country, from the first day
 153 with at least 50 infections. Figure 1 shows N_{jump} for the 137 countries in common to the two data sets;
 154 there are 237 countries in the WHO data set and 139 in the C19CCTF data. It is clear that most countries
 155 have fewer jumps or drops in the Wikipedia data set than in the WHO data set.

156 Thus, at least for the purposes of understanding intrinsic and administrative clustering, the
 157 C19CCTF *medical cases chart* data appear to be the better curated version of the national daily
 158 SARS-CoV-2 infection counts as reported by official agencies. The detailed download and extraction
 159 script of national daily SARS-CoV-2 infection data from these templates and the resulting data file
 160 zenodo.5261231/WP_C19CCTF_SARSCoV2.dat (downloaded 6 May 2021) are available in the repro-
 161 ducibility package associated with this paper (§Code availability). Dates without data are omitted; this
 162 should have an insignificant effect on the analysis if these are due to low infection counts.

163 Another global collection of daily SARS-CoV-2 counts that could be considered is the John Hopkins
 164 University Center for Systems Science and Engineering (JHU CSSE) git repository. Unfortunately, for
 165 several countries, the JHU CSSE data are provided for sub-national divisions rather than as official na-
 166 tional statistics, making the dataset inhomogeneous for the purposes of this study. Artificial interference
 167 in the data at the national level will not be shown in data that is the sum of data obtained directly from
 168 sub-national geographical/political divisions. Moreover, detailed data provenance analysis (which exact
 169 government URL did a particular count come from? where is the archived version of the data of the
 170 original URL?) appears to be more difficult for the JHU CSSE data than for the C19CCTF data. Never-
 171 theless, for completeness, the JHU CSSE data is analysed using the same method as the main analysis,
 172 with results presented as tables in Appendix A.

173 The full set of C19CCTF data includes many days, especially for countries or territories (as defined
 174 by the data source) of low populations, with low values, including zero and one. The standard deviation
 175 of a Poisson distribution (Poisson, 1837) of expectation value N is \sqrt{N} , giving a fractional error of $1/\sqrt{N}$.
 176 Even taking into account clustering or anticlustering of data, inclusion of these periods of close to zero
 177 infection counts would contribute noise that would overwhelm the signal from the periods of higher
 178 infection rates for the same or other countries. In the time sequences of SARS-CoV-2 infection counts,
 179 chaos in the administrative reactions to the initial stages of the pandemic will tend to create extra noise,
 180 so it is reasonable to choose a moderately high threshold at which the start and end of a consecutive
 181 sequence of days should be defined for analysis. Here, we set the threshold for a sequence to start as a
 182 minimum of 50 infections in a single day. The sequence is continued for at least 7 days (if available in
 183 the data), and stops when the counts drop below the same threshold for 2 consecutive days. The cutoff
 184 criterion of 2 consecutive days avoids letting the analysable sequence be too sensitive to individual days

185 of low fluctuations. If the resulting sequence includes less than 7 days, the sequence is rejected as having
186 insufficient signal to be analysed.

187 2.2 RSF Press Freedom Index

188 The *Reporters sans frontières* (RSF) Press Freedom Index is derived annually from an 87-
189 question survey translated into 20 languages and sent to ‘media professionals, lawyers and sociologists’
190 from 180 countries, yielding scores on six general criteria of media freedom and a weighted
191 score representing executions, imprisonments, kidnappings and related abuses against journalists
192 (Reporters sans frontières, 2021). The scores are combined into an overall score from zero (best) to
193 100 (worst) that we denote here as PFI^{2020} .

194 In the absence of artificial interference in the SARS-CoV-2 daily counts, there is no obvious reason
195 why media freedom should relate to the noise in the SARS-CoV-2 counts. However, a correlation be-
196 tween the lack of media freedom and the publication of manipulated data by government agencies would
197 not be surprising. Governments and the public service as organisations, and the individuals that compose
198 them, are under more pressure to be honest in places and epochs where there is more press freedom. To
199 see if the hypothesis of artificial interference is credible, the results of the current work are compared
200 with PFI^{2020} , as published for 2020⁴, in §3.3.

201 2.3 Primary analysis

202 2.3.1 Poissonian and ϕ'_i models: full sequences

203 We first consider the full count sequence $\{n_i(j), 1 \leq j \leq T_i\}$ for each country i , with T_i valid days of
204 analysis as defined in §2.1. Our one-parameter model assumes that the counts are predominantly grouped
205 in clusters, each with ϕ'_i infections per cluster. Thus, the daily count $n_i(j)$ is assumed to consist of
206 $n_i(j)/\phi'_i$ infection events. We assume that $n_i(j)/\phi'_i$ on a given day is drawn from a Poisson distribution
207 of mean $\hat{\mu}_i(j)/\phi'_i$. We set $\hat{\mu}_i(j)$ to the median of the 4 neighbouring days, excluding day j and centred on
208 it. For the initial sequence of 2 days, $\hat{\mu}_i(j)$ is set to $\hat{\mu}_i(3)$, and $\hat{\mu}_i(j)$ for the final 2 days is set to $\hat{\mu}_i(T_i - 2)$.
209 By modelling $\hat{\mu}_i$ as a median of a small number of neighbouring days, our model is almost identical to
210 the data itself and statistically robust, with only mild dependence on the choices of parameters. This
211 definition of a model is more likely to bias the resulting analysis towards underestimating the noise on
212 scales of several days rather than overestimating it; this method will not detect oscillations on the time
213 scale of a few days to a fortnight that are related to the SARS-CoV-2 incubation time (Lauer et al. 2020;
214 Yang et al. 2020, Huang et al. 2020a). For any given value ϕ'_i , we calculate the cumulative probability P'_{ij}
215 that $n_i(j)/\phi'_i$ is drawn from a Poisson distribution of mean $\hat{\mu}_i(j)/\phi'_i$. For country i , the values P'_{ij} should
216 be drawn from a uniform distribution if the model is a fair approximation. In particular, for ϕ'_i set to unity,
217 P'_{ij} should be drawn from a uniform distribution if the intrinsic data distribution is Poissonian. Individual
218 values of P'_{ij} (those that are close to zero or one) could, in principle, be used to identify individual days
219 that are unusual, but here we do not consider these further.

220 We allow a wide logarithmic range in values of ϕ'_i , allowing the unrealistic subrange of $\phi'_i < 1$,
221 and find the value ϕ_i that minimises the Kolmogorov–Smirnov (KS) distance (Kolmogorov 1933;
222 Smirnov 1948; Justel et al. 1997; Marsaglia et al. 2003) from a uniform distribution, i.e. that maximises
223 the KS probability that the data are consistent with a uniform distribution, when varying ϕ'_i . The one-
224 sample KS test is a non-parametric test that compares a data sample with a chosen theoretical probability
225 distribution, yielding the probability that the sample is drawn randomly from the theoretical distribution.
226 This test uses information from the whole of the reconstructed cumulative distribution function, i.e. the
227 set of P'_{ij} values for a given country i . We label the corresponding KS probability as P_i^{KS} . We write
228 $P_i^{Pois} := P_i^{KS}(\phi'_i = 1)$ to check if any country’s daily infection rate sequence is consistent with Poisso-
229 nian, although this is likely to be rare, as stated above: super-Poissonian behaviour seems reasonable. Of
230 particular interest are countries with low values of ϕ_i . Allowing for a possibly fractal or other power-law
231 nature of the clustering of SARS-CoV-2 infection counts, we consider the possibility that the optimal
232 values ϕ_i may be dependent on the total infection count N_i . We investigate the (ϕ_i, N_i) distribution and
233 see whether a scaling type relation exists, allowing for a corrected statistic ψ_i to be defined in order to
234 highlight the noise structure of the counts independent of the overall scale N_i of the counts.

235 Standard errors in ϕ_i for a given country i are estimated once ϕ_i has been obtained by assuming
236 that $\hat{\mu}_i(j)$ and ϕ_i are correct and generating 30 Poisson random simulations of the full sequence for that

⁴<https://rsf.org/en/ranking/2020>, downloaded 4 May 2021

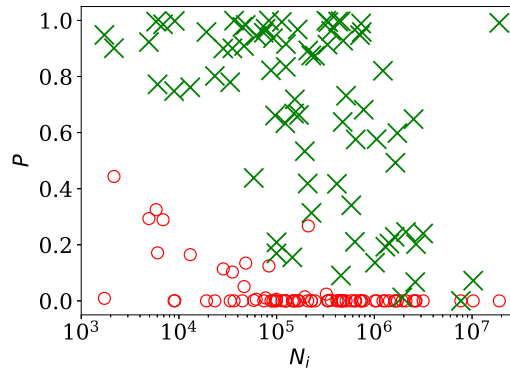


Figure 2. Probability of the noise in the country-level daily SARS-CoV-2 counts being consistent with a Poisson point process, P_i^{Pois} , shown as red circles; and probability $P_i^{\text{KS}}(\phi_i)$ for the ϕ_i clustering model proposed here (§2.3.1), shown as green X symbols; versus N_i , the total number of officially recorded infections for that country. The horizontal axis is logarithmic. As discussed in the text (§3.2.1), the Poisson point process is unrealistic for most of these data, while the ϕ_i clustering model is consistent with the data for most countries. Plain-text table: zenodo.5261231/phi_N_full.dat.

237 country. Since the scales of interest vary logarithmically, the standard deviation of the best estimates of
 238 $\log_{10} \phi_i$ for these numerical simulations is used as an estimate of $\sigma(\log_{10} \phi_i)$, the logarithmic standard
 239 error in ϕ_i .

240 **2.3.2 Subsequences**

241 Since artificial interference in daily SARS-CoV-2 infection counts for a given country might be restricted
 242 to shorter periods than the full data sequence, we also analyse 28-, 14- and 7-day subsequences. These
 243 analyses are performed using the same methods as above (§2.3.1), except that the 28-, 14- or 7-day
 244 subsequence that minimises ϕ_i is found. The search over all possible subsequences would require calcula-
 245 tion of a Šidák-Bonferonni correction factor (Abdi, 2007) to judge how anomalous they are. The KS
 246 probabilities that we calculate need to be interpreted keeping this in mind. Since the subsequences for a
 247 given country overlap, they are clearly not independent from one another. Instead, the *a posteriori* inter-
 248 pretation of the results of the subsequence searches found here should at best be considered indicative of
 249 periods that should be considered interesting for further verification.

250 **2.4 Alternative analyses**

251 Alternatives to the method presented in §2.3.1 are checked to see if they provide better models of the
 252 data.

253 **2.4.1 Logarithmic median model**

254 Each country's time series is by default modelled with the mean of the expected Poisson distribution
 255 for $n_i(j)/\phi_i'$ on a given day being $\hat{\mu}_i(j)/\phi_i'$, where $\hat{\mu}_i(j)$ is the median of n_i in the 4 neighbouring
 256 days, excluding day j and centred on it. As an alternative, we replace $\hat{\mu}_i(j)$ on day j by $\hat{v}_i(j) :=$
 257 $\exp(\text{median}(\ln(n_i)))$ calculated over the same set of neighbouring days. That is, we replace the usual
 258 linear median by a logarithmic median. This might better model the growing and decaying exponential
 259 phases of the infection count sequence.

260 **2.4.2 Negative binomial model**

The negative binomial distribution forbids underdispersion, but is worth considering, given its epi-
 epidemiological motivation for the step from primary to secondary infections (Lloyd-Smith et al. 2005;
 Endo et al. 2020; He et al. 2020). For the counts of a given country i , we define an overdispersion pa-
 rameter ω_i' , where the binomial probability mass function for a given infection count k , considered as k

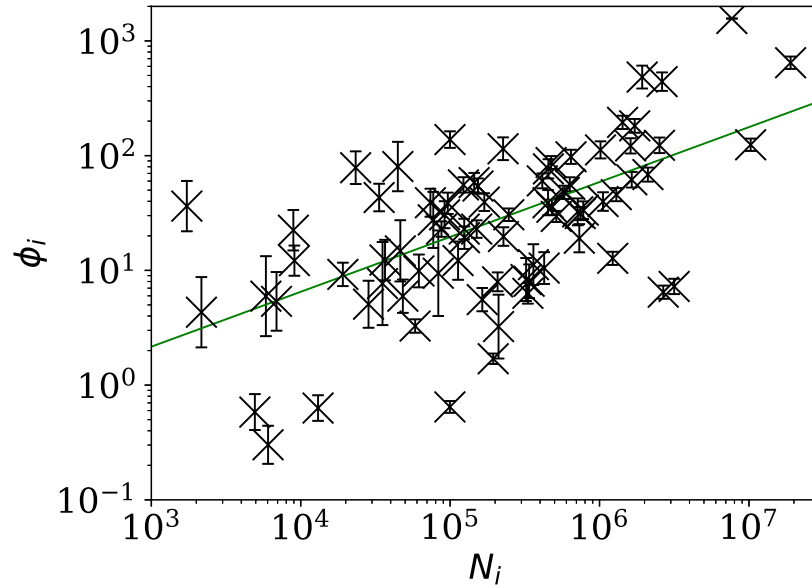


Figure 3. Noisiness in daily SARS-CoV-2 counts, showing the clustering parameter ϕ_i (§2.3.1) that best models the noise, versus the total number of counts for that country N_i . The error bars show standard errors derived from numerical simulations based on the model. The axes are logarithmic, as indicated. Values of the clustering parameter ϕ_i below unity indicate sub-Poissonian behaviour – the counts in these cases are less noisy than expected for Poisson statistics. A robust (Theil, 1950; Sen, 1968) linear fit of $\log_{10} \phi_i$ against $\log_{10} N_i$ is shown as a thick green line (§3.2.1). Plain-text table: [zenodo.5261231/phi_N_full.dat](https://zenodo.org/record/5261231/files/phi_N_full.dat).

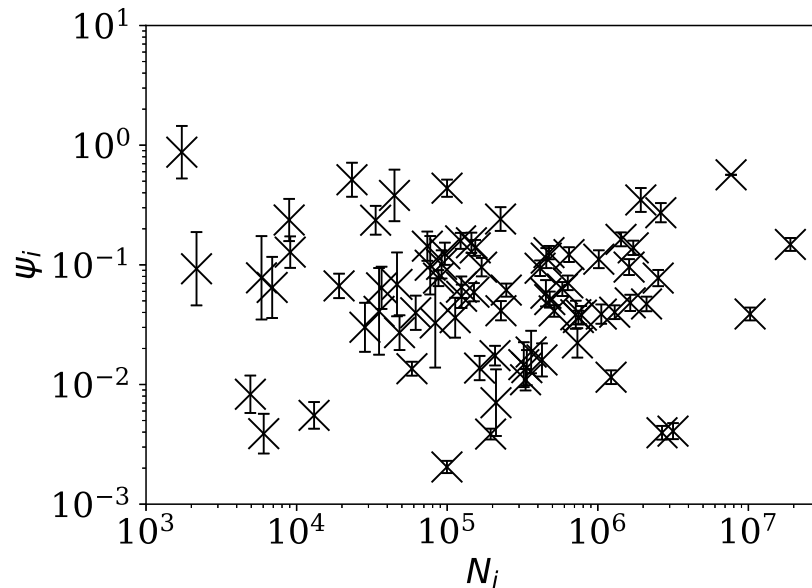


Figure 4. Normalised noisiness ψ_i (Eq. (6)) for daily SARS-CoV-2 counts versus total counts N_i . The error bars are as in Fig. 3, assuming no additional error source contributed by N_i . The axes are logarithmic. Several low ψ_i values appear to be outliers of the ψ_i distribution.

‘failures’, compared to r ‘successes’, with a probability p of success, is

$$P(k; n, p) = \binom{k+r-1}{k} (1-p)^k p^r \quad (1)$$

$$p := \frac{\omega'_i}{1 + \omega'_i}. \quad (2)$$

On day j , with a modelled count of $\hat{\mu}_i(j)$, we set

$$r := \omega'_i \hat{\mu}_i(j), \quad (3)$$

261 giving $\hat{\mu}_i(j)$ as the mean of the distribution and $\hat{\mu}_i(j)(1 + \omega'_i)$ as the variance. The preferred value of
 262 ω'_i (that yielding the lowest Kolmogorov–Smirnov test statistic when comparing the set of cumulative
 263 probabilities with a uniform distribution, as in §2.3.1) is then ω_i . Thus, ω_i should behave similarly to ϕ_i
 264 to represent typical cluster size when both are greater than unity, while at low values (below unity), ω_i
 265 will be unable to represent distributions that are underdispersed with respect to the Poisson distribution,
 266 and will instead rapidly approach zero (the Poisson limit).

267 **2.4.3 Does anti-clustering exist in grouped data?**

268 The temptation to make ‘unnoticeable’ modifications that hide an increase in data from day j to day $j + 1$
 269 might be less likely to occur on greater timescales. Moreover, some of the phenomena contributing to the
 270 intrinsic and administrative components of ϕ'_i should be independent of time scale, while others should
 271 depend on the time scale. To provide clues for this type of analysis, the $n_i(j)$ data have been summed in
 272 pairs and triplets of days, ignoring any one- or two-day remainder at the end of a sequence. These were
 273 analysed using the same algorithm as above for the full sequences (§2.3.1).

274 **2.4.4 Akaike and Bayesian information criteria**

In each case we calculate the Akaike (1974) and Bayesian (Schwarz, 1978) information criteria, defined

$$\text{AIC} := 2k - 2 \sum_i \ln L_i \quad (4)$$

$$\text{BIC} := \ln(N^{\text{days}}) k - 2 \sum_i \ln L_i, \quad (5)$$

275 respectively. The number of free parameters k is defined as the number of countries satisfying the criteria
 276 for a sequence to be analysable (§2.1), since there is one free parameter allowed to vary individually for
 277 each country. The number of data points for BIC is set to the total number of days N^{days} in the sequences
 278 over all k countries. The ϕ'_i model, and the logarithmic median and negative binomial alternatives, each
 279 have the same values of k and N^{days} . The 2-day and 3-day alternatives can be expected to have slightly
 280 smaller numbers of countries k whose sequences satisfy the analysis criteria, and much smaller numbers
 281 N^{days} of ‘days’, since in reality these no longer represent single days. The maximum likelihood is
 282 defined $L_i := P_i^{\text{KS}}$, i.e. the Kolmogorov–Smirnov probability that the observed values for the country are
 283 drawn from a rescaled Poisson (or negative binomial) distribution, as defined above.

284 **3 RESULTS**

285 **3.1 Data**

286 The 139 countries and territories in the C19CCTF counts data have 27 negative values out of the total
 287 of 36445 values. These can reasonably be interpreted as corrections for earlier overcounts, and we reset
 288 these values to zero, with a negligible reduction in the amount of data. Consecutive sequences of days
 289 satisfying the criteria listed in §2.1 were found for $M^{\text{valid}} = 78$ countries.

290 **3.2 Clustering of SARS-CoV-2 counts**

291 **3.2.1 Full infection count sequences**

292 Figure 2 shows, unsurprisingly, that only a small handful of the countries’ daily SARS-CoV-2 counts
 293 sequences have noise whose statistical distribution is consistent with the Poisson distribution, in the
 294 sense modelled here: P_i^{Pois} (red circles) is close to zero in most cases. Specifically, 63 countries (80.8%)
 295 are inconsistent with the Poisson distribution at a significance of $P_i^{\text{Pois}} < 0.01$ and 66 countries (84.6%)

Table 1. Clustering parameters for the countries with the 10 lowest ϕ_i and 10 lowest ψ_i values, i.e. the least noise; extended version of table: zenodo.5261231/phi_N_full.dat.

country	ϕ'_i model					alternative analyses			
	N_i	P_i^{Poiss}	P_i^{KS}	ϕ_i	ψ_i	\hat{v}_i	ω_i	P_i^{KS}	ω_i
Nicaragua	6046	0.17	0.77	0.30	0.003	0.66	0.30	0.17	0.00
Syria	4931	0.29	0.92	0.58	0.008	0.92	0.58	0.29	0.00
Tajikistan	13062	0.17	0.76	0.63	0.005	0.78	0.67	0.16	0.00
Algeria	99610	0.01	0.17	0.65	0.002	0.13	0.62	0.01	0.00
Belarus	194284	0.01	0.53	1.70	0.003	0.40	1.57	0.46	0.58
Croatia	210837	0.27	0.89	3.24	0.007	0.89	3.24	0.70	1.02
Albania	58316	0.00	0.44	3.27	0.013	0.41	3.27	0.30	1.80
New Zealand	2164	0.44	0.90	4.32	0.092	0.94	4.32	0.86	1.19
Australia	28430	0.11	0.90	5.07	0.030	0.90	5.69	0.87	3.55
Thailand	6884	0.29	0.99	5.37	0.064	0.99	5.37	0.96	3.80
Algeria	99610	0.01	0.17	0.65	0.002	0.13	0.62	0.01	0.00
Belarus	194284	0.01	0.53	1.70	0.003	0.40	1.57	0.46	0.58
Nicaragua	6046	0.17	0.77	0.30	0.003	0.66	0.30	0.17	0.00
Turkey	2669568	0.00	0.20	6.46	0.003	0.16	6.09	0.16	5.07
Russia	3159297	0.00	0.24	7.24	0.004	0.19	7.08	0.22	6.03
Tajikistan	13062	0.17	0.76	0.63	0.005	0.78	0.67	0.16	0.00
Croatia	210837	0.27	0.89	3.24	0.007	0.89	3.24	0.70	1.02
Syria	4931	0.29	0.92	0.58	0.008	0.92	0.58	0.29	0.00
Saudi Arabia	331359	0.00	0.91	6.31	0.010	0.84	6.17	0.83	4.90
Iran	1225142	0.00	0.82	12.73	0.011	0.58	11.61	0.71	11.35

are non-Poissonian at $P_i^{\text{Poiss}} < 0.05$. On the contrary, the introduction of the ϕ'_i parameter, optimised to ϕ_i for each country i , provides a sufficiently good fit in most cases, especially for the countries with low clustering ϕ_i . While some of the probabilities ($P_i^{\text{KS}}(\phi_i)$, green x symbols) in Fig. 2 are low in countries with the highest numbers of infections, these countries also have high ϕ_i , so are not of interest as indicators of the absence of noise. Among countries with $\phi_i < 10.0$, the lowest probability P_i^{KS} is that of Algeria with $P_i^{\text{KS}} = 0.17$, i.e., the ϕ_i model is consistent with the data. In contrast, the negative binomial model ϕ_i^{NB} (see §3.2.3 below), which is super-Poissonian by definition, and cannot model sub-Poissonian behaviour, yields $P_i^{\text{KS}} = 0.01$ for Algeria. Consistently with this, the Poissonian model for Algeria gives $P_i^{\text{Poiss}} = 0.005$. The full sequence for Algeria is only fit by the ϕ'_i model, which allows sub-Poissonian behaviour.

The consistency of the ϕ_i model with most of the data justifies continuing to Figure 3, which clearly shows a scaling relation: countries with greater overall numbers N_i of infections also tend to have greater noise in the daily counts $n_i(j)$. A Theil–Sen linear fit (Theil, 1950; Sen, 1968) to the relation between $\log_{10} \phi_i$ and $\log_{10} N_i$ has a zeropoint of -1.10 ± 0.44 and a slope of 0.48 ± 0.07 , where the standard errors (68% confidence intervals if the distribution is Gaussian) are conservatively generated for both slope and zeropoint by 100 bootstraps. By using a robust estimator, the low ϕ_i cases, which appear to be outliers, have little influence on the fit. The fit is shown as a thick green line in Fig. 3.

This ϕ_i – N_i relation is consistent with $\phi_i \propto \sqrt{N_i}$. To adjust the ϕ_i clustering value to take into account the dependence on N_i , and given that the slope is consistent with this simple relation, we propose an empirical definition of a normalised clustering parameter

$$\psi_i := \phi_i / \sqrt{N_i}, \quad (6)$$

so that ψ_i should, by construction, be approximately constant. While the estimated slope of the relation could be used rather than this half-integer power relation, the fixed relation in Eq. (6) offers the benefit of simplicity.

This relation should not be confused with the usual Poisson error. By the divisibility of the Poisson

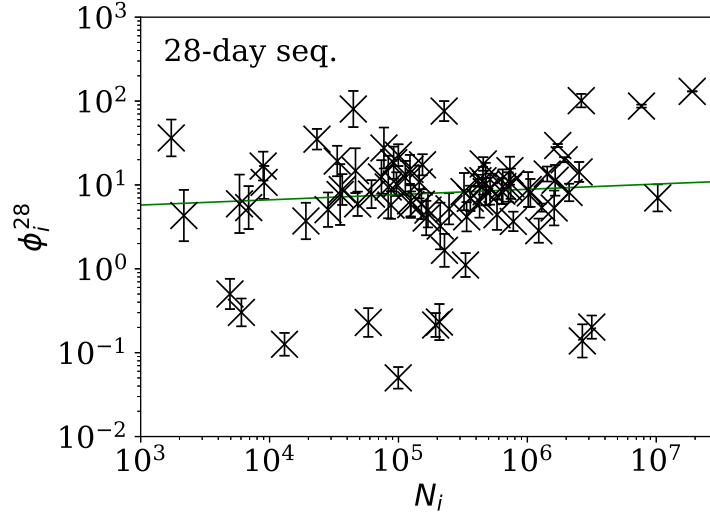


Figure 5. Clustering parameter ϕ_i^{28} for the 28-day sequence of lowest ϕ_i^{28} , as in Fig. 3. The vertical axis range is expanded from that in Fig. 3, to accommodate lower values. A robust (Theil, 1950; Sen, 1968) linear fit of $\log_{10} \phi_i^{28}$ against $\log_{10} N_i$ is shown as a thick green line (§3.2.1). Plain-text table: zenodo.5261231/phi_N_28days.dat.

distribution, the relation $\phi_i \propto \sqrt{N_i}$ that was found here can be used to show that

$$\begin{aligned} \sigma[\hat{\mu}_i(j)/\phi_i] &\sim \sqrt{\hat{\mu}_i(j)/\phi_i} \\ \Rightarrow \sigma[\hat{\mu}_i(j)] &\sim \phi_i \sqrt{\hat{\mu}_i(j)/\phi_i} \propto N_i^{1/4} \hat{\mu}_i(j)^{1/2}, \end{aligned} \quad (7)$$

where $\sigma[x]$ is the standard deviation of random variable x . If we accept $\hat{\mu}_i(j)$ as a fair model for $n_i(j)$ and that $n_i(j)$ is proportional to N_i , then we obtain

$$\sigma[n_i(j)] \propto n_i^{3/4}. \quad (8)$$

316 Figure 4 shows visually that ψ_i appears to be scale-independent, in the sense that the dependence on
317 N_i has been cancelled, by construction. The countries with the 10 lowest values of ψ_i are Algeria, Belarus,

Table 2. Least noisy 28-day sequences – clustering parameters for the countries with the 10 lowest ϕ_i^{28} values; extended table: zenodo.5261231/phi_N_28days.dat.

country	N_i	$\langle n_i^{28} \rangle$	P_i^{Poiss}	P_i^{KS}	ϕ_i^{28}	starting date
Algeria	99610	227.6	0.00	0.36	0.05	2020-09-03
Tajikistan	13062	63.0	0.02	0.96	0.13	2020-06-07
Turkey	2669568	1014.5	0.03	1.00	0.14	2020-06-30
Russia	3159297	5403.8	0.26	0.59	0.20	2020-07-20
Belarus	194284	921.9	0.14	0.89	0.21	2020-05-08
Albania	58316	203.8	0.33	0.64	0.23	2020-09-27
United Arab Emirates	207822	512.8	0.08	0.23	0.23	2020-04-14
Nicaragua	6046	135.7	0.17	0.77	0.30	2020-07-07
Syria	4931	70.0	0.19	0.91	0.50	2020-08-15
Saudi Arabia	331359	1182.2	0.47	0.54	1.11	2020-04-12

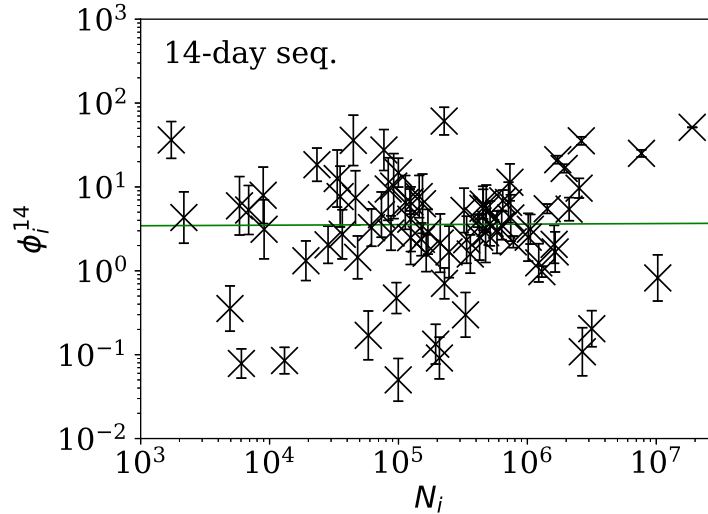


Figure 6. Clustering parameter ϕ_i^{14} for the 14-day sequence of lowest ϕ_i^{14} , as in Fig. 5. Plain-text table: zenodo.5261231/phi_N_14days.dat.

318 Nicaragua, Turkey, Russia, Tajikistan, Croatia, Syria, Saudi Arabia, and Iran. Detailed SARS-CoV-2
 319 daily count noise characteristics for the countries with lowest ϕ_i and ψ_i are listed in Table 1, including
 320 the Kolmogorov–Smirnov probability that the data are drawn from a Poisson distribution, P_i^{Poiss} , the
 321 probability of the optimal ϕ_i model, P_i^{KS} , and ϕ_i and ψ_i .

322 The approximate proportionality of ϕ_i to $\sqrt{N_i}$ for the full sequences is strong and helps separate
 323 low-noise SARS-CoV-2 count countries from those following the main trend. However, the results for
 324 subsequences shown below in §3.2.2 suggest that this N_i dependence may be an effect of the typically
 325 longer durations of the pandemic in countries where the overall count is higher.

3.2.2 Subsequences of infection counts

326 Figures 5–7 show the equivalent of Fig. 3 for sequences of lengths 28, 14 and 7 days, respectively.
 327 The Theil–Sen robust fits to the logarithmic (ϕ_i^{28}, N_i) ; (ϕ_i^{14}, N_i) ; and (ϕ_i^7, N_i) relations are zeropoints
 328 and slopes of 0.57 ± 0.43 and 0.06 ± 0.08 ; 0.52 ± 0.47 and 0.01 ± 0.09 ; and -0.10 ± 0.83 and $0.02 \pm$
 329 0.13 , respectively. There is clearly no significant dependence of ϕ_i^d on N_i for any of these fixed length
 330 subsequences, in contrast to the case of the ϕ_i dependence on N_i for the full count sequences. Thus,
 331

Table 3. Least noisy 14-day sequences – clustering parameters for the countries with the 10 lowest ϕ_i^{14} values; extended version of table: zenodo.5261231/phi_N_14days.dat.

country	N_i	$\langle n_i^{14} \rangle$	P_i^{Poiss}	P_i^{KS}	ϕ_i^{14}	starting date
Algeria	99610	285.9	0.12	0.40	0.05	2020-09-01
Nicaragua	6046	73.6	0.12	0.98	0.08	2020-09-22
Tajikistan	13062	64.6	0.02	0.99	0.09	2020-06-11
United Arab Emirates	207822	521.2	0.11	0.56	0.09	2020-04-19
Turkey	2669568	971.6	0.12	0.86	0.11	2020-07-08
Belarus	194284	945.6	0.22	1.00	0.13	2020-05-12
Albania	58316	143.4	0.21	0.96	0.17	2020-09-01
Russia	3159297	5627.0	0.47	0.98	0.20	2020-07-21
Saudi Arabia	331359	1227.5	0.38	0.96	0.30	2020-04-19
Syria	4931	76.6	0.42	0.96	0.35	2020-08-14

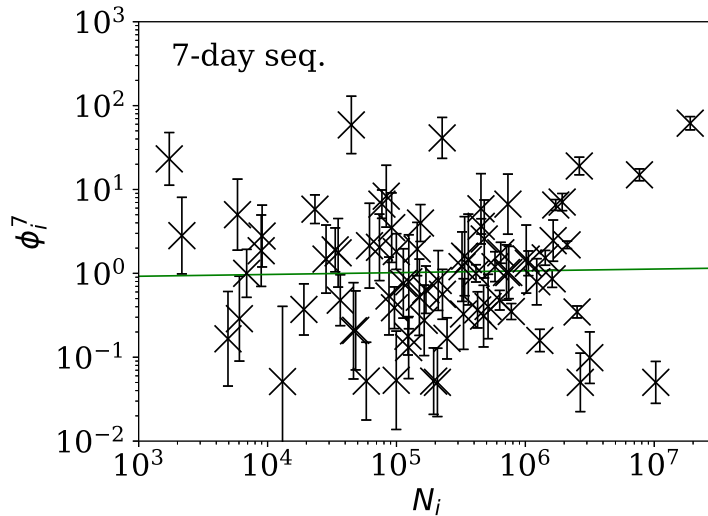


Figure 7. Clustering parameter ϕ_i^7 for the 7-day sequence of lowest ϕ_i^7 , as in Fig. 5. There are clearly a wider overall scatter and bigger error bars compared to Figs 5 and 6; a low ϕ_i^7 is a noisier indicator than ϕ_i^{28} and ϕ_i^{14} for individual countries. Plain-text table: zenodo.5261231/phi_N_07days.dat.

Table 4. Least noisy 7-day sequences – clustering parameters for the countries with the 10 lowest ϕ_i^7 values; extended table: zenodo.5261231/phi_N_07days.dat.

country	N_i	$\langle n_i^7 \rangle$	P_i^{Poiss}	P_i^{KS}	ϕ_i^7	starting date
United Arab Emirates	207822	544.9	0.24	0.99	0.05	2020-04-27
India	10266674	10109.3	0.34	0.60	0.05	2020-06-06
Turkey	2669568	929.6	0.22	0.93	0.05	2020-07-15
Tajikistan	13062	51.9	0.16	0.77	0.05	2020-06-28
Albania	58316	297.7	0.23	0.98	0.05	2020-10-18
Belarus	194284	947.9	0.60	0.94	0.05	2020-05-13
Algeria	99610	204.3	0.37	0.49	0.05	2020-10-14
Russia	3159297	5076.7	0.36	0.68	0.10	2020-08-09
Ethiopia	124264	456.7	0.83	0.93	0.13	2020-12-13
Poland	1294878	297.7	0.31	0.96	0.16	2020-06-20

Table 5. Akaike (1974) and Bayesian (Schwarz, 1978) information criteria for the ϕ'_i and alternative analyses; plain-text version: zenodo.5261231/AIC_BIC_full.dat.

model	ϕ'_i		log. median		neg. binomial		2-day grouping		3-day grouping	
	AIC	BIC	AIC	BIC	AIC	BIC	AIC	BIC	AIC	BIC
	268.60	848.87	289.91	870.18	377.52	957.79	313.21	878.50	208.49	743.75

Table 6. Kendall τ statistic and its significance (two-sided) P^τ for the null hypothesis of no correlation between the ranking of PFI²⁰²⁰ and ϕ_i or ψ_i for the full data or subsequences; plain-text version: zenodo.5261231/pfi_correlations_table.dat.

parameter	full		28-day		14-day		7-day	
	τ	P^τ	τ	P^τ	τ	P^τ	τ	P^τ
ϕ_i	-0.118	0.131	-0.126	0.108	-0.148	0.0584	-0.200	0.0108
ψ_i	-0.160	0.0408	-0.157	0.0445	-0.176	0.0249	-0.170	0.0300

332 the empirical motivation for using ψ_i (Eq. (6)) to discriminate between the countries' full sequences of
 333 SARS-CoV-2 data is not justified from the information gained from the subsequences alone. Tables 2–4
 334 show the countries with the least noisy sequences as determined by ϕ_i^{28} , ϕ_i^{14} and ϕ_i^7 , respectively.

335 Tables 2 and 3 show that the lists of countries with the strongest anti-clustering are similar to one
 336 another. Thus, Fig. 8 shows the SARS-CoV-2 counts curves for countries with the lowest ϕ_i^{28} , and Fig. 9
 337 the curves for those with the lowest ϕ_i^7 . Both figures exclude countries with total counts $N_i \leq 10000$, in
 338 which low total counts tend to give low clustering. It is clear in these figures that several countries have
 339 subsequences that are strongly sub-Poissonian – with some form of anti-clustering, whether natural or
 340 artificial.

341 Countries in the median of the ϕ_i^{28} and ϕ_i^7 distributions have their curves shown in Fig. 10 for com-
 342 parison. It is visually clear in the figure that the counts are dispersed widely beyond the Poissonian band,
 343 and that the ϕ_i^{28} and ϕ_i^7 models are reasonable as a model for representing about 68% of the counts
 344 within one standard deviation of the model values.

345 **3.2.3 Alternative analyses**

346 Figure 11 (left) shows that the logarithmic median model (§2.4.1) of the counts gives almost identical
 347 best estimates to those of the primary model, i.e. $\psi_i^{LM} \approx \psi_i$, but Table 5 shows very strong evidence
 348 favouring the original, arithmetic median model.

349 Figure 11 (right) shows that the negative binomial model (§2.4.2) roughly gives $\psi_i^{NB} \sim \psi_i$ (i.e. $\omega_i \sim$
 350 ϕ_i), tending to $\psi_i^{NB} < \psi_i$, especially for the least clustered cases. The error bars are very big for ψ_i^{NB}
 351 for several countries. Table 5 again shows very strong evidence favouring the original model over the
 352 negative binomial model.

353 Figure 12 shows that the counts grouped (summed) in pairs and triplets (§2.4.3) yield ψ_i^{2d} and ψ_i^{3d}
 354 with more scatter and generally larger error bars than that of ψ_i , and ψ_i^{2d} and ψ_i^{3d} are mostly greater
 355 than ψ_i . Whether the AIC and BIC evidence (Table 5) for 2-day and 3-day grouped data can be di-
 356 rectly compared to that of the main analysis depends on whether the grouped data can be considered
 357 to be the same observational data as the original data, modelled with fewer free parameters. Since the
 358 characteristic of study is the noise, not the signal, the validity of this direct comparison is doubtful. Nev-
 359 ertheless, if the values of the AIC and BIC evidence are considered literally, then the 2-day grouping
 360 would yield a worse model than the model of the daily data, while the 3-day grouping would yield a
 361 better model than that for the daily data. The comparison of these different analyses could potentially
 362 be used to obtain a deeper understanding of the complex dynamics of this pandemic. The epidemio-
 363 logically relevant sociological parameters of countries around the world are highly diverse (varying in
 364 population density, patterns of social contact, tendency to obey or disobey official health guidelines such
 365 as lockdown measures, demographic profiles, quality and availability of health services, communication
 366 patterns, frequency of COVID-19 comorbidity conditions, climate (Afshordi et al., 2020)), so compari-

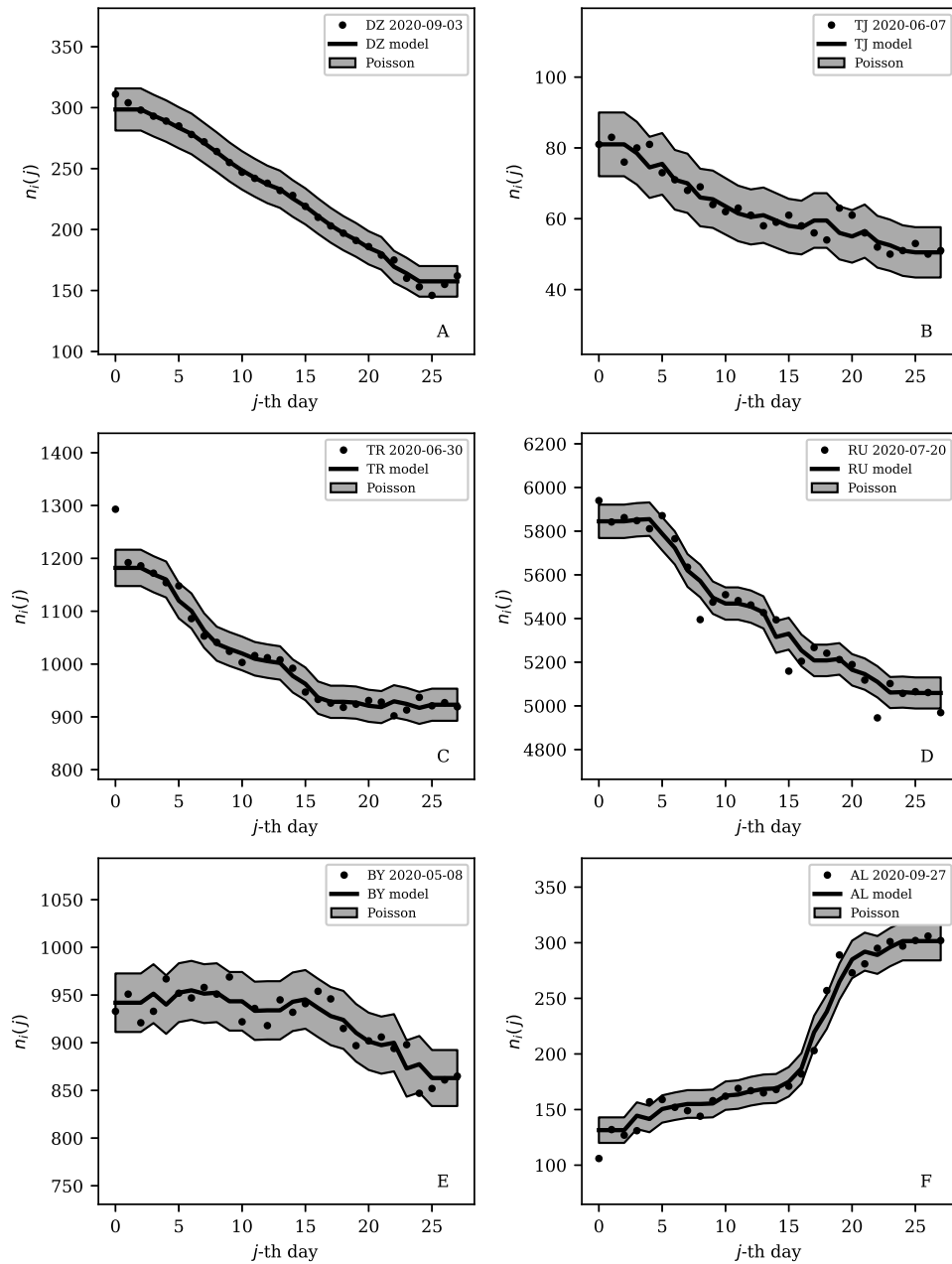


Figure 8. Least noisy 28-day official SARS-CoV-2 national daily counts for countries with total counts $N_i > 10000$ (see Fig. 5 and Table 2), shown as dots in comparison to the $\hat{\mu}_i(j)$ model (median of the 4 neighbouring days) and 68% error band for the Poisson point process. The ranges in daily counts (vertical axis) are chosen automatically and in most cases do not start at zero. About nine (32%) of the points should be outside of the shaded band unless the counts have an anti-clustering effect that weakens Poisson noise. The dates indicate the start date of each sequence. ISO-3166-1 key: *A*: DZ: Algeria, *B*: TJ: Tajikistan, *C*: TR: Turkey, *D*: RU: Russia, *E*: BY: Belarus, *F*: AL: Albania.

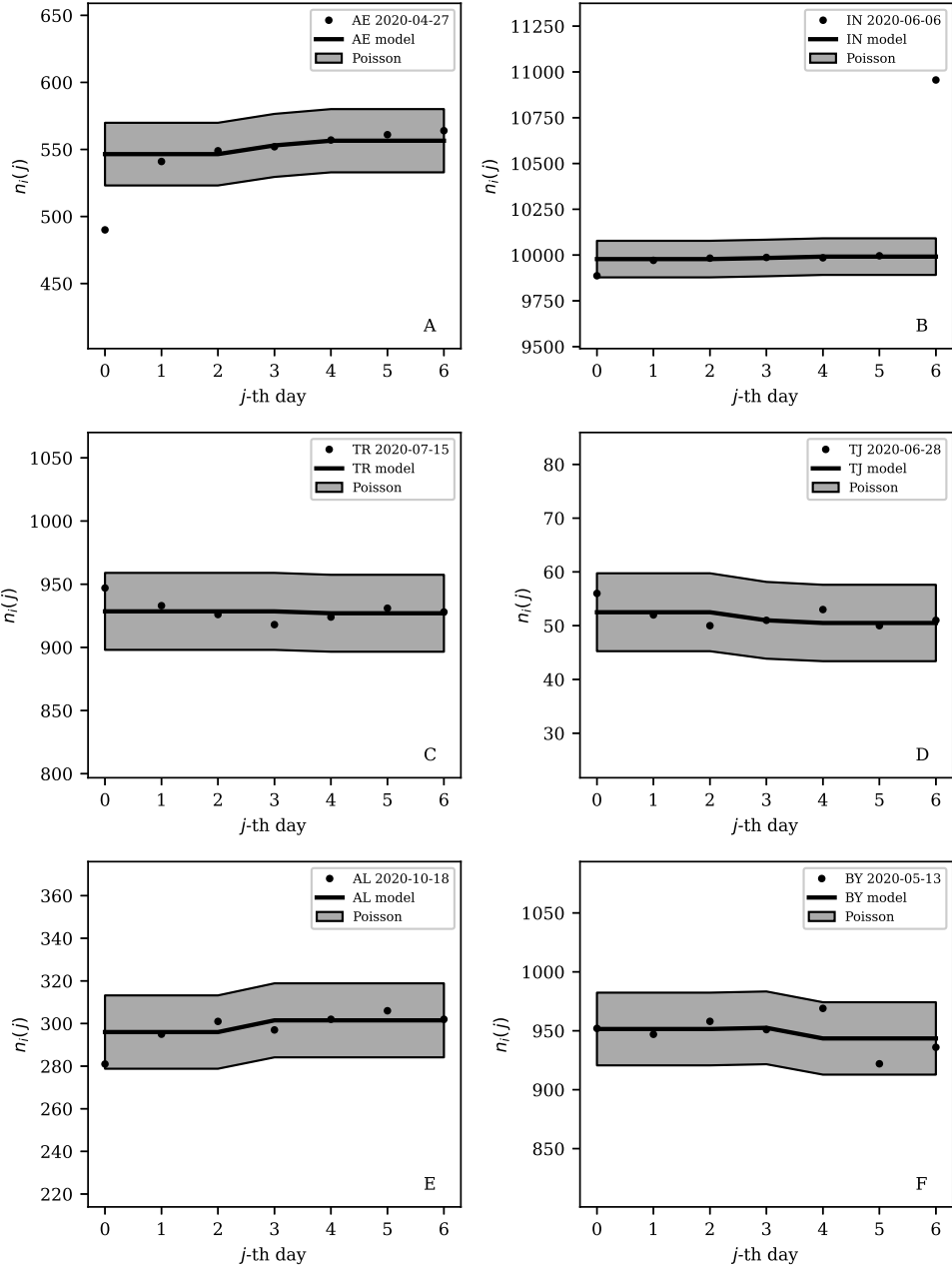


Figure 9. Least noisy 7-day daily counts for countries with total counts $N_i > 10000$ (see Fig. 7 and Table 4), as in Fig. 8. A concentration of points close to the model indicates an anti-clustering effect; about 68% (five) of the points should scatter up and down throughout the shaded band if the counts are Poissonian, and about 32% (two) should be outside the band. In several cases, the data points appear to be mostly stuck to the model, with almost no scatter. ISO-3166-1 key: *A*: AE: United Arab Emirates, *B*: IN: India, *C*: TR: Turkey, *D*: TJ: Tajikistan, *E*: AL: Albania, *F*: BY: Belarus.

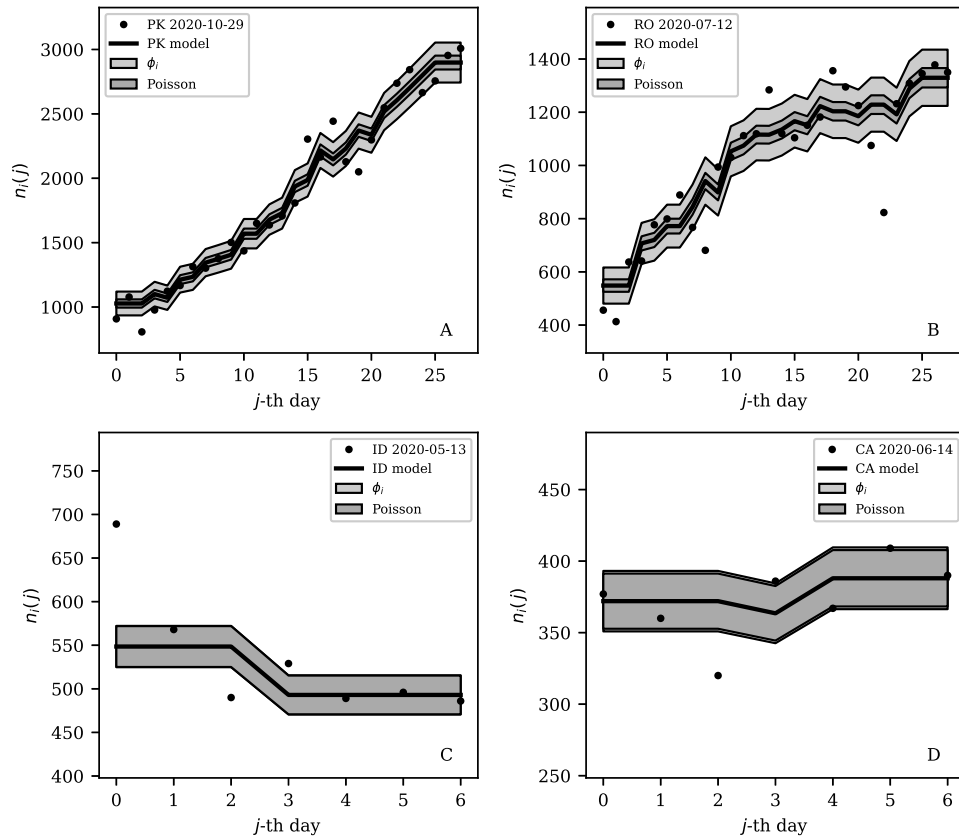


Figure 10. Typical (median) 28-day (above) and 7-day (below) daily counts, as in Figs 8 and 9. The dark shaded band again shows a Poissonian noise model, which underestimates the noise. A faint shaded band shows the ϕ_i models for these countries' SARS-CoV-2 daily counts, and should contain about 68% of the infection count points. ISO-3166-1 key: A: PK: Pakistan, B: RO: Romania, C: ID: Indonesia, D: CA: Canada.

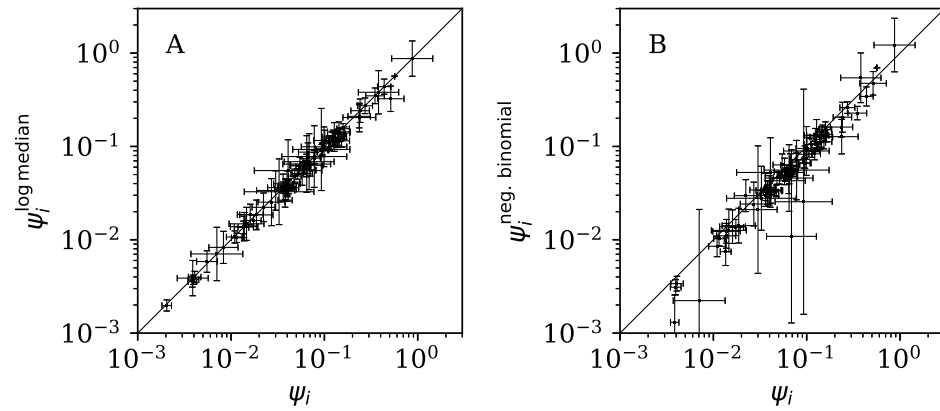


Figure 11. *A:* Normalised clustering parameter ψ_i^{LM} (Eq. (6)) using the logarithmic median model of the expected full-sequence counts (§2.4.1) versus ψ_i for the primary analysis. *B:* Normalised clustering parameter $\psi_i^{\text{NB}} := \omega_i/\sqrt{N_i}$ for the negative binomial model (see Eqs (2), (3)) versus ψ_i . A line shows $\psi_i^{\text{LM}} = \psi_i$ and $\psi_i^{\text{NB}} = \psi_i$, respectively. The data point for Algeria, with $\log_{10} \psi_i = -2.69 \pm 0.05$, $\log_{10} \psi_i^{\text{NB}} = -5.69 \pm 0.93$, lies below the displayed area in the right-hand panel. Plain-text table: zenodo.5261231/phi_N_full.dat.

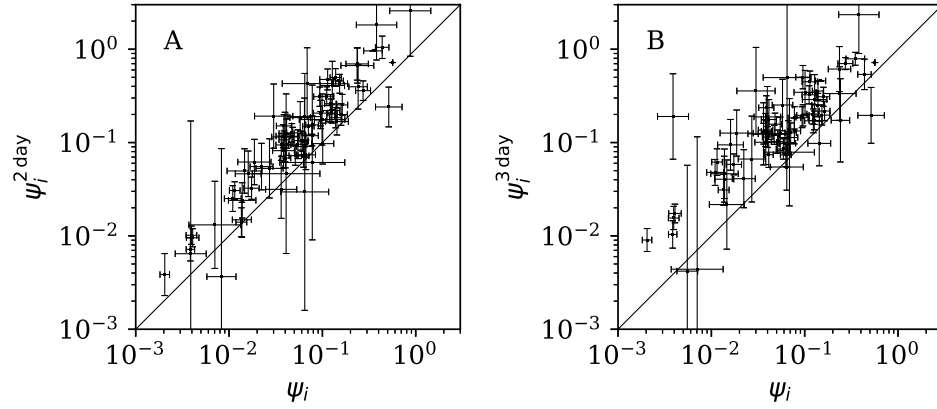


Figure 12. Normalised noisiness ψ_i^{2d} and ψ_i^{3d} (Eq. (6)) for counts summed in successive pairs (A) and triplets (B) of days, respectively, versus that for the primary analysis. A line shows $\psi_i^{2d} = \psi_i$ and $\psi_i^{3d} = \psi_i$, respectively. Plain-text table: zenodo.5261231/phi_N_full.dat.

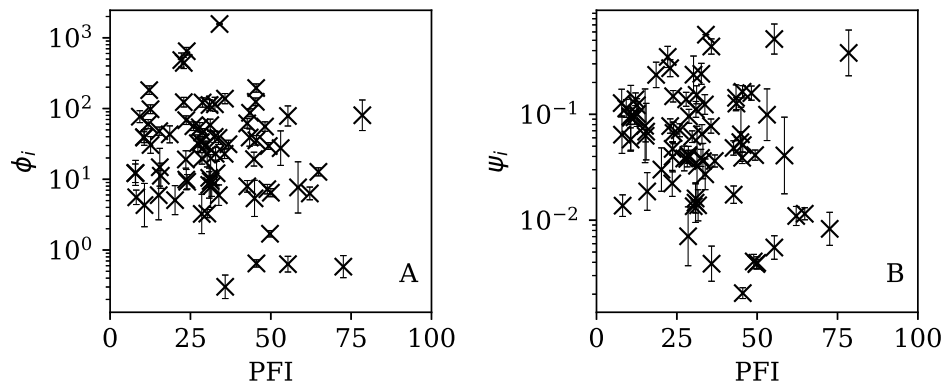


Figure 13. Dependence of ϕ_i (left: A) and ψ_i (right: B) on the Press Freedom Index (PFI²⁰²⁰) for the full sequences. The vertical axis ranges in these two panels and through to Fig. 16 differ from one another.

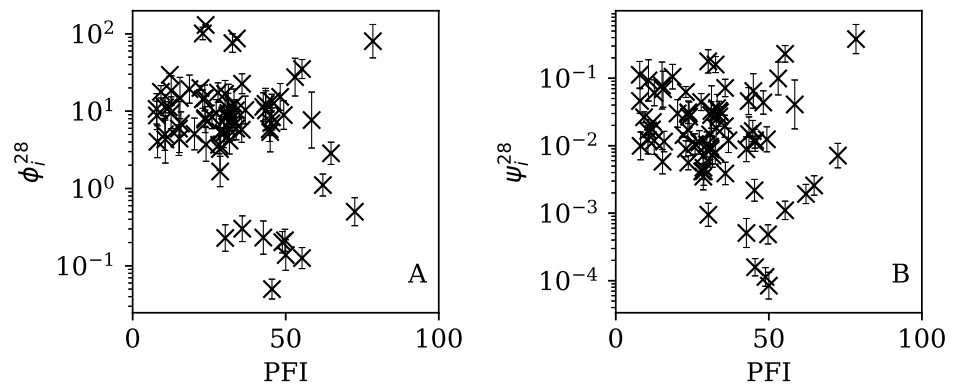


Figure 14. Dependence of ϕ_i^{28} (A) and ψ_i^{28} (B) on PFI^{2020} for the 28-day subsequences.

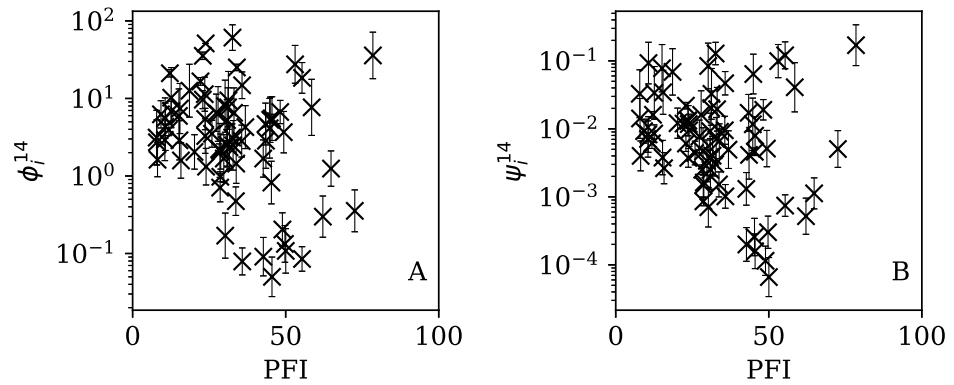


Figure 15. Dependence of ϕ_i^{14} (A) and ψ_i^{14} (B) on PFI^{2020} for the 14-day subsequences.

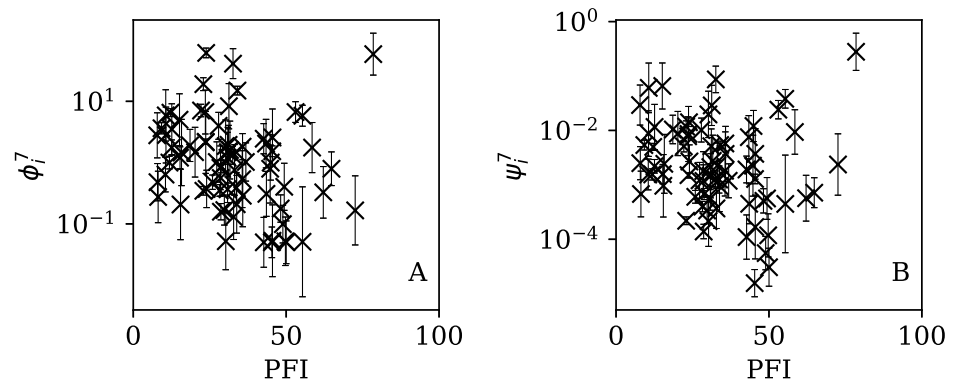


Figure 16. Dependence of ϕ_i^7 (A) and ψ_i^7 (B) on PFI^{2020} for the 7-day subsequences.

367 son of the clustering behaviour on these different time scales might help to separate out some of these
368 contributions.

369 **3.3 Comparison with the RSF Press Freedom Index**

370 Figures 13–16 show the relation between ϕ_i and ψ_i and the RSF Press Freedom Index (PFI²⁰²⁰; §2.2) for
371 the full sequences and subsequences. Table 6 non-parametrically tests for correlations in these relations
372 using the Kendall rank correlation statistic τ (Kendall 1938; Kendall 1970; Croux & Dehon 2010). The
373 first row of the table shows that the unnormalised clustering parameter ϕ_i for the full sequence and
374 subsequences generally anticorrelates with PFI²⁰²⁰. The strongest case is for 7-day subsequences, in
375 which case the anticorrelation is significant at $P^\tau = 0.0108$.

376 The normalised clustering parameter ψ_i was found to be necessary above (Eq. (6)) to remove depen-
377 dence on the total infection scale N_i in the full sequences. The second row of Table 6 shows that for ψ_i ,
378 the anticorrelation is significant at the $P^\tau < 0.05$ level for the full sequence ($P^\tau = 0.0408$) and for all
379 the subsequences. However, the analysis of the subsequence results (§3.2.2) only justifies considering
380 ψ_i as the preferred parameter for the full sequence, and using ϕ_i^{28} , ϕ_i^{14} , and ϕ_i^7 for the subsequences.
381 Together, ψ_i , ϕ_i^{28} , ϕ_i^{14} , and ϕ_i^7 yield a median significance level of $P^\tau = 0.0496 < 0.05$ (the significance
382 is stronger in the JHU CSSE data; see the corresponding table in Appendix A). Thus, there is statistically
383 significant evidence that the worse the press freedom is in a country (as measured by higher PFI²⁰²⁰), the
384 more likely it is that the SARS-CoV-2 daily counts are best modelled as sub-Poissonian.

385 This result is an anticorrelation; it is not proof of a causal relation. Nevertheless, a simple explanation
386 of the observed relation would be that there is interference in the data in association with a lack of media
387 freedom.

388 **4 DISCUSSION**

389 Figures 3–7 vary in the degree to which they separate some groups of countries as being unusual in terms
390 of the characteristics of their location in the (N_i, ψ_i) plane. On visual inspection, Fig. 5, for ϕ_i^{28} , appears
391 to show the sharpest division between the main relation between clustering and total infection count, in
392 which nine countries appear to have sub-Poissonian preferred models in a group well-separated from the
393 others. If we interpret the sub-Poissonian behaviour as a result of interference associated with the lack
394 of media freedom (high PFI²⁰²⁰, §3.3, Table 6), then the more significant results are those for ϕ_i^7 (Fig. 7,
395 Table 4). If interference did occur, then other public evidence of interference might add credibility to the
396 interpretation. Here, some possible interpretations are discussed, including some individual low-noise
397 sequences in Fig. 8 and 9. Some typical sequences (as selected by median ϕ_i^{28} and ϕ_i^7) are shown for
398 comparison in Fig. 10.

399 The analysis in this paper makes very few assumptions and does not claim to measure the full na-
400 ture of the pandemic. The following interpretations of the numerical results would benefit from future
401 studies that attempt worldwide models of the underlying epidemiology of the pandemic. Detailed mod-
402 elling is usually restricted to a small number of countries (e.g. Chowdhury et al. 2020; Kim et al. 2020;
403 Molina-Cuevas 2020; Jiang, Zhao & Shao 2021; Afshordi et al. 2020).

404 **4.1 High total infection count**

405 While the main question of interest in this paper is whether anti-clustering can be detected, the results
406 may also indicate characteristics of countries with high clustering values. The United States, India and
407 Brazil are clearly separated in Figs 3 and 4 from the majority of other countries by their high official
408 total infection counts of about 10^7 . They have correspondingly higher clustering values ϕ_i , although
409 their normalised clustering values ψ_i are in the range of about $0.01 < \psi_i < 1$ covered by the majority of
410 countries in Fig. 4.

411 It does not seem realistic that the ϕ_i values greater than 600 for the US and Brazil are purely an effect
412 of intrinsic infection events – ‘superspreader’ events in crowded places or nursing homes. While individ-
413 ual big clusters may occur given the high overall scale of infections, it seems more likely that there is a
414 strong role played by administrative clustering. Both countries are federations, and have numerous geo-
415 graphic administrative subdivisions with a diversity of political and administrative methods. A plausible
416 explanation for the dominant effect yielding $\phi_i > 600$ in these two countries is that on any individual day,
417 the arrival and full processing of reports depends on a number of sub-national administrative regions,
418 each reporting a few hundred new infections.

419 For example, if there are 100 reporting regions, with typically about 10 of these each reporting about
 420 600 infections daily, then typically (on about 68% of days) there will be about 7 to 13 reports per day.
 421 This would give a range varying from about 4200 to 7800 cases per day, rather than 5923 to 6077,
 422 which would be the case for unclustered, Poissonian counts (since $\sqrt{6000} \approx 77$). Lacking a system that
 423 obliges sub-national divisions – and laboratories – to report their test results in time-continuous fashion
 424 and that validates and collates those reports on a time scale much shorter than 24 hours, this type of
 425 clustering seems natural in the sociological sense. It is also possible that in these two large federations,
 426 the intrinsic heterogeneity compared to many countries of smaller populations leads to other noise effects
 427 that combine with the ‘administrative’ effect of stochasticity in the number of regional reports received
 428 as sketched above.

429 India’s overall position in the (ψ_i, N_i) plane (Fig. 4 and Table 1) appears quite typical, with an un-
 430 normalised clustering parameter $\phi_i = 124.45 \times 10^{\pm 0.054}$. However, Table 4 shows that despite its large
 431 overall infection count, India achieved a 7-day sequence with a preferred $\phi_i^7 = 0.05$, giving it a place in
 432 Table 4 and being easy to identify in the bottom-right part of Fig. 7. Figure 9 presents this subsequence.
 433 Five values appear almost exactly on the model curve rather than scattering above and below. More-
 434 over, the value is just below 10,000. Epidemiologically, it is not credible to believe that 10,000 officially
 435 reported cases per day should be an attractor resulting from the pattern of infections and system of report-
 436 ing. Given that the value of 10,000 is a round number in the decimal-based system, a reasonable specu-
 437 lation would be that the daily counts for India were artificially held at just below 10,000 for several days.
 438 The crossing of the 10,000 psychological threshold of daily infections was noted in the media (Porecha,
 439 2020), but the lack of noise in the counts during the week preceding the crossing of the threshold appears
 440 to have gone unnoticed. After crossing the 10,000 threshold, the daily infections in India continued in-
 441 creasing, as can be seen in the full counts (zenodo.5261231/WP_C19CCTF_SARSCoV2.dat).

442 4.2 Neither Poissonian nor super-Poissonian

443 The negative binomial model ϕ_i^{NB} (§3.2.3) rejects the possibility of Algeria having a super-Poissonian
 444 noise distribution at $P_i^{\text{KS}} = 0.01$. The Poissonian model for Algeria is similarly rejected with $P_i^{\text{Poiss}} =$
 445 0.005 . However, the ϕ_i model does model the Algeria data adequately, with a modest probability of
 446 $P_i^{\text{KS}} = 0.17$.

447 Figure 8 dramatically shows the least noisy 28-day sequence for Algeria. Only two days of SARS-
 448 CoV-2 recorded infections during this period appear to have diverged towards the edge of the Poissonian
 449 68% band, rather than about nine, the expected number that should be outside this band for a Poisso-
 450 nian distribution. Almost all of the points appear to stick extremely closely to the median model. It
 451 is difficult to imagine a natural process for obtaining noise that is this strongly sub-Poissonian, espe-
 452 cially in the context where most countries have super-Poissonian daily counts. Compartmental epi-
 453 demic modelling of the Algerian data, which has been published for the period ending 24 May 2020
 454 (Rouabah, Tounsi & Belaloui, 2020), could be used to try to reconstruct the true daily counts.

455 4.3 Low normalised clustering ψ_i or subsequence clustering ϕ_i^{28}, ϕ_i^{14} , or ϕ_i^7

456 4.3.1 Low clustering, high N_i

457 Turkey and Russia have total infection counts of about 3 million, similar to those of several other coun-
 458 tries, but have managed to keep their daily infection rates much less noisy – by about a factor of 10 to
 459 100 – than would be expected from the general pattern displayed in the figures. These two countries
 460 appear as an isolated pair in the bottom-right of both Figs 4 and 5, and appear in all four tables of low ψ_i
 461 (Table 1) and low subsequence ϕ_i (Tables 2–4). Russia has the very modest value of $\phi_i = 7.24 \times 10^{\pm 0.067}$
 462 and Turkey has $\phi_i = 6.46 \times 10^{\pm 0.057}$, despite their large total infection counts. This would require that
 463 both intrinsic clustering of infection events and administrative procedures work much more smoothly in
 464 Russia and Turkey than in other countries with comparable total infection counts. Tables 2 and 3 and
 465 Fig. 8 show that the Russian and Turkish official SARS-CoV-2 counts indeed show very little noise com-
 466 pared to more typical cases (Fig. 10). There appear to be weekend dips in the Russian case (see §4.3.4
 467 below). Since these are included in the analysis, an exclusion of the weekend dips would lead to an even
 468 lower clustering estimate. At the intrinsic epidemiological level, if the Russian and Turkish counts are
 469 to be considered accurate, then very few clusters – in nursing homes, religious gatherings, bars, restau-
 470 rants, schools, shops – can have occurred. Moreover, laboratory testing and transmission of data through
 471 the administrative chain from local levels to the national health agency must have occurred without the

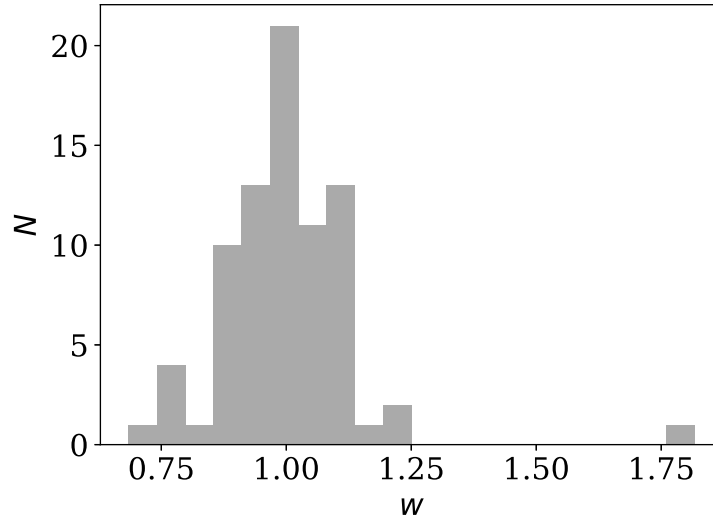


Figure 17. Histogram of weekly dip w_i (Eq. (9)) in national daily SARS-CoV-2 counts. Values below unity indicate a dip; values above unity indicate a bump. Plain-text full list of w_i : [zenodo.5261231/phi_N_full.dat](https://zenodo.org/record/5261231/files/phi_N_full.dat).

472 clustering effects that are present in the data for the United States, Brazil, India, and other countries
 473 with high total infection counts $N_i > 2$ million, for which ϕ_i is typically above 100. International me-
 474 dia interest in Russian COVID-19 data has mostly focussed on controversy related to COVID-19 death
 475 counts (Cole, 2020), with apparently no attention given so far to the modestly super-Poissonian nature
 476 of the daily counts, in contrast to the strongly super-Poissonian counts of other countries with high total
 477 infection counts. How did Russia and Turkey achieve low ϕ_i (super-Poissonian), i.e. low clustering?

478 **4.3.2 Low clustering, medium N_i**

479 Some cases of interest appear among the countries with officially lower total infection counts. The
 480 Belarus (BY) case is present in all four tables (Tables 1–4). The least noisy Belarusian counts curve
 481 appears in Figs 8 and 9. As with the other panels in the daily counts figures, the vertical axis is set by the
 482 data instead of starting at zero, in order to best display the information on the noise in the counts. With the
 483 vertical axis starting at zero, the Belarus daily counts would look nearly flat in this figure. They appear to
 484 be bounded above by the round number of 1000 SARS-CoV-2 infections per day, which, again, as in the
 485 case of India, could appear to be a psychologically preferred barrier. Media have expressed scepticism
 486 of Belarusian COVID-19 related data (Kramer, 2020; AFN, 2020). The Albanian case (Figs 8 and 9)
 487 also could be interpreted as hitting a psychological barrier of a decimal round number, an artificial cap
 488 of 300 infections per day, in mid-October 2020.

489 One remaining case of a coincidence is that the lowest noise 7-day sequence listed for Poland (Ta-
 490 ble 4) is for the 7-day period starting 20 June 2020, with $\phi_i^7 = 0.16 \times 10^{\pm 0.13}$. This is a factor of about
 491 300 below Poland’s clustering value for the full sequence of its SARS-CoV-2 daily infection counts,
 492 $\phi_i = 45.71 \times 10^{\pm 0.057}$, which Fig. 3 shows is typical for a country with an intermediate total infection
 493 count. On 28 June 2020, there was a *de facto* (of disputed constitutional validity, Wyrzykowski 2020;
 494 Letowska & Pacewicz 2020) first-round presidential election in Poland. Figure 9 shows that the counts
 495 for Poland during the final pre-first-round-election week did not scatter widely throughout the Poisso-
 496 nian band. A decimal-system round number also appears in this figure: the daily infection rate is slightly
 497 above about 300 infections per day and drops to slightly below that. This appears to be the same psycho-
 498 logical daily infection count attractor as for Albania. The intrinsic clustering of SARS-CoV-2 infections
 499 in Poland together with testing and administrative clustering of the confirmed cases appear to have tem-
 500 porarily disappeared just prior to the election date, yielding what is best modelled as an incident of
 501 sub-Poissonian counts.

502 **4.3.3 JHU CSSE data**

503 The JHU CSSE data give mostly similar results to the C19CCTF data. These are presented and briefly
504 discussed in Appendix A.

505 **4.3.4 Weekend dips in the counts**

One sociological contribution to noise not mentioned above is that in several countries, the official daily counts are lower on or immediately after weekends. Credible factors include fewer medical and laboratory workers available to carry out tests and fewer administrators registering, collecting and transmitting data. A dip in the counts on weekends would tend to add noise to the daily count time series, making the above results conservative. These dips can be quantified using the one-dimensional discrete fast Fourier transform (FFT). With the usual FFT convention, we transform $n_i(j)$ into $f_i(j)$ at j days, where $f_i(0)$ is the mean and a weekly dip should appear as a negative value at $f_i(7)$. We define a ‘weekend dip’ w_i for country i by subtracting the mean of the neighbours and normalising:

$$w_i := 1 + \pi \frac{f_i(7) - [f_i(6) + f_i(8)]/2}{f_i(0)}. \quad (9)$$

506 This should correspond to a multiplicative factor, i.e., $w_i = 0.85$ means a 15% dip.

507 Figure 17 shows the distribution of w_i (mean \pm std. error: 1.001 ± 0.015 ; std. dev.: 0.137; median:
508 0.999; interquartile range: 0.104). Unexpectedly, not only are there several countries with dips, but
509 there are also several countries with a strong *excess* signal on the 7-day time scale. There is no reason
510 to expect the overall distribution to be Gaussian. The Shapiro–Wilk statistic (Shapiro & Wilk, 1965) is
511 $W = 0.806$, rejecting the possibility of the distribution being Gaussian to extremely high significance:
512 $p = 9.82 \times 10^{-9}$. Future work in studying the noise characteristics of a pandemic could take into account
513 this weekly component of daily infection statistics.

514 **4.4 Further statistical models: autoregression**

515 A possible extension of the current work would be to iteratively consider an autoregressive model (e.g.,
516 Papoulis & Pillai 2002, §12-3; Fokianos & Tjøstheim 2011; Agosto et al. 2021) for each time series. An
517 initial model such as the one used here, the median of the preceding and succeeding days, could first be
518 inferred from the sequence. This would be subtracted from the time series $n_i(j)$ to obtain a process that
519 could be assumed as having a stationary central value and a time-varying noise distribution. An autore-
520 gressive model of the resulting sequence (or its logarithm) could then be modelled by a time-dependent
521 (j -dependent) Poissonian or negative binomial stochastic term to find the optimal autoregression coeffi-
522 cients. The resulting coefficients could then be used to subtract an improved model from the times series
523 and obtain a new iteration of an autoregression model. Continuing the iteration might lead to conver-
524 gence on a specific autoregressive model that is stable against further iteration. In this case, the residual
525 noise could then be analysed as in the current work. Alternatively, time series analysis of SARS-CoV-2
526 counts allowing time-varying trends (Harvey & Kattuman, 2020) could be carried out prior to analysing
527 the properties of the noise itself, as in this work.

528 **4.5 RSF Press Freedom Index**

529 Although the relations in Fig 13–16 generally show anticorrelations (PFI²⁰²⁰ increases from 0 to 100 as
530 press freedom decreases, i.e. it could be better described as a lack-of-press-freedom parameter), there
531 does appear to be a tendency for the countries with the lowest clustering values to have intermediate
532 PFI²⁰²⁰ \sim 40. In other words, despite the overall relation, some countries with the lowest levels of press
533 freedom appear to have noise in their daily SARS-CoV-2 counts that appears only moderately low or
534 typical. Mainland China stands out as an exception in all eight panels of these four figures, with both a
535 high clustering, $\phi_i = 80.35$ in the full sequence case, and a high lack of press freedom, PFI²⁰²⁰ = 78.48.

536 While a causal relation, via general processes of media freedom pressuring politicians and pub-
537 lic servants to produce honest data, and vice versa, would provide the simplest interpretation of the
538 overall correlation found here, other interpretations should be considered. Indices to measure the
539 much wider concept of democracy tend to suffer from a lack of clarity in definitions and method
540 (Munck & Verkuilen, 2002), quite likely due to the nature of democracy as a highly complex phe-
541 nomenon that is difficult to represent with a single index. Nevertheless, Balashov et al. (2021) study
542 the relations between democracy indicators and validity in daily COVID-19 data, using a very different

543 method to the one introduced in this paper, and point out that democracy, economic and health system
544 national indicators tend to correlate strongly to one another (see §2 of Balashov et al. 2021 for a liter-
545 ature review of relations between democracy and data manipulation). An alternative interpretation to
546 direct causality could be explored along these lines. Other lines of analysis would be needed to establish
547 causal relations instead of statistical correlations.

548 5 CONCLUSION

549 Given the overdispersed, one-parameter Poissonian ϕ_i model proposed, the noise characteristics of the
550 daily SARS-CoV-2 infection data suggest that most of the countries' data form a single family in the
551 (ϕ_i, N_i) plane. The clustering – whether epidemiological in origin, or caused by testing or administrative
552 pipelines – tends to be greater for greater numbers of total infections. Several countries appear, however,
553 to show unusually anti-clustered (low-noise) daily infection counts.

554 Since these daily infection counts data constitute data of high epidemiological interest, the statistical
555 characteristics presented here and the general method could be used as the basis for further investi-
556 gation into the data of countries showing exceptional characteristics. The relations between the most
557 anti-clustered counts and the psychologically significant decimal system round numbers (India: 10,000
558 daily, Belarus: 1000 daily, Albania, Poland: 300 daily), and in relation to a *de facto* national presidential
559 election, raise the question of whether or not these are just coincidences. A statistically significant anti-
560 correlation of the clustering with the *Reporters sans frontières* Press Freedom Index was found, i.e., less
561 press freedom was found to correlate with less clustering, strengthening the credibility of the ϕ_i cluster-
562 ing model for judging the validity of daily pandemic data published by national government agencies.
563 The suspicious periods of data found here are mostly complementary to those studied by Balashov et al.,
564 since those authors' Benford's law analysis mainly focuses on the first-digit Benford's law during the
565 exponentially growing phases of the pandemic in any particular country (Balashov et al., 2021), while
566 this analysis studies noise in data for the full pandemic up to 6 May 2021.

567 It should be straightforward for any reader to extend the analysis in this paper by first checking
568 its reproducibility with the free-licensed source package provided using the MANEAGE framework
569 (Akhlaghi et al., 2021), and then extending, updating or modifying it in other appropriate ways; see
570 §Code availability below. Reuse of the data should be straightforward using the files archived at
571 zenodo.5261231.

572 **ACKNOWLEDGEMENTS** Thank you to Marius Peper, Taha Rouabah, Dmitry Borodaenko, anonymous col-
573 leagues, and to Niayesh Afshordi and the two other referees for several useful comments and to the Maneage
574 developers for the Maneage framework in general and for several specific comments on this work. This project used
575 computing resources of the Poznań Supercomputing and Networking Center (PSNC) provided under computational
576 grant 314.

577 **SOFTWARE ACKNOWLEDGEMENTS** This research was partly done using the following free-licensed soft-
578 ware packages: Boost 1.73.0, Bzip2 1.0.6, cURL 7.71.1, Dash 0.5.10.2, Discoteq flock 0.2.3, Eigen 3.3.7, Expat
579 2.2.9, File 5.39, Fontconfig 2.13.1, FreeType 2.10.2, Git 2.28.0, GNU Autoconf 2.69.200-babc, GNU Automake
580 1.16.2, GNU AWK 5.1.0, GNU Bash 5.0.18, GNU Binutils 2.35, GNU Compiler Collection (GCC) 10.2.0, GNU
581 Coreutils 8.32, GNU Diffutils 3.7, GNU Findutils 4.7.0, GNU gettext 0.21, GNU gperf 3.1, GNU Grep 3.4, GNU
582 Gzip 1.10, GNU Integer Set Library 0.18, GNU libiconv 1.16, GNU Libtool 2.4.6, GNU libunistring 0.9.10, GNU
583 M4 1.4.18-patched, GNU Make 4.3, GNU Multiple Precision Arithmetic Library 6.2.0, GNU Multiple Precision
584 Complex library, GNU Multiple Precision Floating-Point Reliably 4.0.2, GNU Nano 5.2, GNU NCURSES 6.2,
585 GNU Patch 2.7.6, GNU Readline 8.0, GNU Sed 4.8, GNU Tar 1.32, GNU Texinfo 6.7, GNU Wget 1.20.3, GNU
586 Which 2.21, GPL Ghostscript 9.52, ImageMagick 7.0.8-67, Less 563, Libbsd 0.10.0, Libffi 3.2.1, libICE 1.0.10,
587 Libidn 1.36, Libjpeg v9b, Libpaper 1.1.28, Libpng 1.6.37, libpthread-stubs (Xorg) 0.4, libSM 1.2.3, Libtiff 4.0.10,
588 libXau (Xorg) 1.0.9, libxcb (Xorg) 1.14, libXdmpc (Xorg) 1.1.3, libXext 1.3.4, Libxml2 2.9.9, libXt 1.2.0, Lzip
589 1.22-rc2, Metastore (forked) 1.1.2-23-fa9170b, OpenBLAS 0.3.10, Open MPI 4.0.4, OpenSSL 1.1.1a, PatchELF
590 0.10, Perl 5.32.0, pkg-config 0.29.2, Python 3.8.5, Unzip 6.0, util-Linux 2.35, util-macros (Xorg) 1.19.2, X11 library
591 1.6.9, XCB-proto (Xorg) 1.14, xorgproto 2020.1, xtrans (Xorg) 1.4.0, XZ Utils 5.2.5, Zip 3.0 and Zlib 1.2.11. Python
592 packages used include: Cyclus 0.10.0, Cython 0.29.21, Kiwisolver 1.0.1, Matplotlib 3.3.0 (Hunter, 2007), Numpy
593 1.19.1 (van der Walt et al., 2011), pybind11 2.5.0, PyParsing 2.3.1, python-dateutil 2.8.0, Scipy 1.5.2 (Oliphant,

594 2007; Millman & Aivazis, 2011), Setuptools 41.6.0, Setuptools-scm 3.3.3 and Six 1.12.0. \LaTeX packages for creat-
595 ing the pdf version of the paper included: algorithmicx 15878 (revision), algorithms 0.1, biber 2.16, biblatex 3.16,
596 bitset 1.3, booktabs 1.61803398, breakurl 1.40, caption 56771 (revision), changepage 1.0c, courier 35058 (revision),
597 csquotes 5.2l, datetime 2.60, dblfloatfix 1.0a, ec 1.0, enumitem 3.9, epstopdf 2.28, eso-pic 3.0a, etoolbox 2.5k, fan-
598 cyhdr 4.0.1, float 1.3d, fntcount 3.07, fontaxes 1.0e, footmisc 5.5b, fp 2.1d, kastrup 15878 (revision), lastpage 1.2m,
599 latexpand 1.6, letltxmacro 1.6, lineno 4.41, listings 1.8d, logreq 1.0, microtype 2.8c, multirow 2.8, mweights 53520
600 (revision), newtx 1.655, pdfescape 1.15, pdftexcmds 0.33, pgf 3.1.9a, pgfplots 1.18.1, preprint 2011, setspace 6.7a,
601 soul 2.4, sttools 2.1, subfig 1.3, tex 3.141592653, texgyre 2.501, times 35058 (revision), titlesec 2.14, trimspaces
602 1.1, txfonts 15878 (revision), ulem 53365 (revision), varwidth 0.92, wrapfig 3.6, xcolor 2.12, xkeyval 2.8 and xstring
603 1.84.

604

605 **FUNDING** No funding has been received for this project.

606 **DATA AVAILABILITY** As described above in §2.1, the source of curated SARS-CoV-2 infec-
607 tion count data used for the main analysis in this paper is the C19CCTF data, downloaded
608 using the script `download-wikipedia-SARS-CoV-2-charts.sh` and stored in the file
609 `Wikipedia_SARSCoV2_charts.dat` in the reproducibility package available at zenodo.5261231. The
610 data file is archived at zenodo.5261231/WP_C19CCTF_SARSCoV2.dat. The WHO data that was compared with
611 the C19CCTF data via a jump analysis (Fig. 1) was downloaded from [https://covid19.who.int/WHO-](https://covid19.who.int/WHO-COVID-19-global-data.csv)
612 `COVID-19-global-data.csv` and was archived on 6 May 2021.

613 **CODE AVAILABILITY** In addition to the SARS-CoV-2 infection count data for this paper, the full download-
614 ing of complementary data, calculations, production of figures, tables and values quoted in the text of the pdf
615 version of the paper are intended to be fully reproducible on any POSIX-compatible system using free-licensed
616 software, which, by definition, the user may modify, redistribute, and redistribute in modified form. The re-
617 producibility framework is technically a GIT branch of the MANEAGE package (Akhlaghi et al., 2021)⁵, earlier
618 used to produce reproducible papers (Infante-Sainz et al., 2020). The GIT repository commit ID of this version
619 of this paper is `subpoisson-e217f39`. The primary (live) GIT repository is [https://codeberg.org/boud/](https://codeberg.org/boud/subpoisson)
620 `subpoisson`, archived at `sw:h:l:rev:eb46500ec25b9584324656d4f3f730cb0fdeba7b`. The full reproducibility
621 package is archived at zenodo.5261231. Bug reports and discussion are welcome at [https://codeberg.org/](https://codeberg.org/boud/subpoisson/issues)
622 `boud/subpoisson/issues`.

623 **CONFLICT OF INTEREST** The author of this paper is aware of no financial or similar conflicts of interests.

624 **ORCID** *Boudewijn F. Roukema* ORCID: <https://orcid.org/0000-0002-3772-0250>

625 REFERENCES

- 626 AFN 2020, Nexta channel accuses the Ministry of Health of the Republic of Belarus of publishing censored data on
627 coronavirus (in Russian), *AFN*, <https://afn.by/news/i/275882>, Archived at Wayback
628 Abdi S., 2007, Bonferroni and Sidak corrections for multiple comparisons. Thousand Oaks, Sage, USA,
629 <https://personal.utdallas.edu/~%7Eherve/Abdi-Bonferroni2007-pretty.pdf>,
630 Archived at Wayback
631 Afshordi N., Holder B., Bahrami M., Lichtblau D., 2020, Diverse local epidemics reveal the distinct effects of
632 population density, demographics, climate, depletion of susceptibles, and intervention in the first wave of COVID-
633 19 in the United States, *arXiv e-prints*, (arXiv:2007.00159)
634 Agosto A., Campmas A., Giudici P., Renda A., 2021, Monitoring COVID-19 contagion growth, *Stat. in Medicine*,
635 1, 11
636 Akaike H., 1974, A new look at the statistical model identification, *IEEE Trans. on Auto. Contr.*, 19, 716
637 Akhlaghi M., Infante-Sainz R., Roukema B. F., Khellat M., Valls-Gabaud D., Baena-Gallé R., 2021, Toward Long-
638 term and Archivable Reproducibility, *Comp. in Sci. Eng.*, 23, 82 (arXiv:2006.03018)

⁵<https://maneage.org>

639 Balashov V. S., Yan Y., Zhu X., 2021, Who Manipulates Data During Pandemics? Evidence from Newcomb-Benford
640 Law, *arXiv e-prints*, (arXiv:2007.14841)

641 Barabási A.-L., 2005, The origin of bursts and heavy tails in human dynamics, *Nature*, 435, 207
642 (arXiv:cond-mat/0505371)

643 Billah A., Miah M., Khan N., 2020, Reproductive number of coronavirus: A systematic review and meta-analysis
644 based on global level evidence, *PLoS One*, 15, e0242128

645 Chowdhury R., Heng K., Shawon M. S. R., Goh G., Okonofua D., Ochoa-Rosales C., Gonzalez-Jaramillo V., Bhuiya
646 A., Reidpath D., Prathapan S., Shahzad S., Althaus C. L., Gonzalez-Jaramillo N., Franco O. H., 2020, Dynamic
647 interventions to control COVID-19 pandemic: a multivariate prediction modelling study comparing 16 worldwide
648 countries, *Eur. J. Epidemiol.*, 35, 389

649 Cole B., 2020, Russia accuses media of false coronavirus death numbers as Moscow officials say 60 percent of
650 fatalities not included, *Newsweek*, [https://www.newsweek.com/russia-accuses-media-false-](https://www.newsweek.com/russia-accuses-media-false-coronavirus-death-numbers-1503932)
651 [coronavirus-death-numbers-1503932](https://www.newsweek.com/russia-accuses-media-false-coronavirus-death-numbers-1503932), Archived at Archive Today

652 Croux C., Dehon C., 2010, Influence functions of the Spearman and Kendall correlation measures,
653 *Stat. Methods Appl.*, 19, 497

654 Endo A., Abbott S., Kucharski A. J., Funk S., 2020, Estimating the overdispersion in COVID-19 transmission using
655 outbreak sizes outside China, *Wellcome Open Res.*, 5, 67

656 Fokianos K., Tjøstheim D., 2011, Log-linear Poisson autoregression, *J. Multivariate Analysis*, 102, 563

657 Goh K.-I., Barabasi A.-L., 2006, Burstiness and Memory in Complex Systems, *Europhys. Lett. Assoc.*, 81, 4
658 (arXiv:physics/0610233)

659 Harvey A., Kattuman P., 2020, Time series models based on growth curves with applications to forecasting coron-
660 avirus, *Harv. Data Sci. Rev.*, DOI:10.1162/99608f92.828f40de

661 He D., Zhao S., Xu X., Lin Q., Zhuang Z., Cao P., Wang M. H., Lou Y., Xiao L., Wu Y., Yang L., 2020, Low
662 dispersion in the infectiousness of COVID-19 cases implies difficulty in control, *BMC Public Health*, 20, 1558

663 Huang L., Zhang X., Zhang X., Zhijian W., Zhang L., Xu J., Liang P., Xu Y., Zhang C., Xu A., 2020a, Rapid asymp-
664 tomatic transmission of COVID-19 during the incubation period demonstrating strong infectivity in a cluster of
665 youngsters aged 16–23 years outside Wuhan and characteristics of young patients with COVID-19: A prospective
666 contact-tracing study, *J. Infection*, 80, e1

667 Huang C., Wang Y., Li X., Ren L., Zhao J., Hu Y., Zhang L., Fan G., Xu J., Gu X., Cheng Z., Yu T., Xia J., Wei Y.,
668 Wu W., Xie X., Yin W., Li H., Liu M., Xiao Y., Gao H., Guo L., Xie J., Wang G., Jiang R., Gao Z., Jin Q., Wang
669 J., Cao B., 2020b, Clinical features of patients infected with 2019 novel coronavirus in Wuhan, China, *Lancet*,
670 395, 97

671 Hunter J. D., 2007, Matplotlib: A 2d graphics environment, *CiSE*, 9, 90

672 Infante-Sainz R., Trujillo I., Román J., 2020, The Sloan Digital Sky Survey extended point spread functions, *MNRAS*,
673 491, 5317 (arXiv:1911.01430)

674 Jiang F., Zhao Z., Shao X., 2021, Time Series Analysis of COVID-19 Infection Curve: A Change-Point Perspective,
675 *J. Econometrics*, in press (arXiv:2007.04553)

676 Johnson N., Kemp A. W., Kotz S., 2005, *Univariate Discrete Distributions* (3rd ed.). John Wiley & Sons, Inc., New
677 York, NY, USA, doi:10.1002/0471715816

678 Justel A., Peña D., Zamar R., 1997, A multivariate Kolmogorov-Smirnov test of goodness of fit, *Stat.Prob.Letters*,
679 35, 251

680 Keegan B. C., Tan C., 2020, A Quantitative Portrait of Wikipedia’s High-Tempo Collaborations during the 2020
681 Coronavirus Pandemic, *arXiv e-prints*, (arXiv:2006.08899)

682 Kendall M. G., 1938, A New Measure of Rank Correlation, *Biometrika*, 30, 81

683 Kendall M. G., 1970, *Rank Correlation Methods*, 4th edn. Griffin, London

684 Kim T., Lieberman B., Luta G., Pena E., 2020, Prediction Regions for Poisson and Over-Dispersed Poisson Regres-
685 sion Models with Applications to Forecasting Number of Deaths during the COVID-19 Pandemic, *arXiv e-prints*
686 , (arXiv:2007.02105)

687 Koch C., Okamura K., 2020, Benford’s Law and COVID-19 reporting, *Econ.Lett.*, 196, 109573

688 Kolmogorov A. N., 1933, Sulla Determinazione Empirica di Una Legge di Distribuzione, *Giornale dell’Istituto*
689 *Italiano degli Attuari*, 4, 83

690 Kramer A. E., 2020, “There Are No Viruses Here”: Leader of Belarus Scoffs at Lockdowns, *The New*
691 *York Times*, [https://www.nytimes.com/2020/04/25/world/europe/belarus-lukashenko-](https://www.nytimes.com/2020/04/25/world/europe/belarus-lukashenko-coronavirus.html)
692 [coronavirus.html](https://www.nytimes.com/2020/04/25/world/europe/belarus-lukashenko-coronavirus.html), Archived at Archive Today

693 Lauer S. A., Grantz K. H., Bi Q., Jones F. K., Zheng Q., Meredith H. R., Azman A. S., Reich N. G., Lessler
694 J., 2020, The Incubation Period of Coronavirus Disease 2019 (COVID-19) From Publicly Reported Confirmed
695 Cases: Estimation and Application, *Ann.Intern.Med.*, M20, 0504

696 Lee K.-B., Han S., Jeong Y., 2020, COVID-19, flattening the curve, and Benford’s law, *Physica A*, 559, 125090

697 Letowska E., Pacewicz P., 2020, Prof. Łętowska: To nie były wybory, ale plebiscyt. Uchybienia wyborcze rzucają
698 długi gęsty cień, *OKO.press*, <https://oko.press/prof-letowska-to-nie-byly-wybory-ale->

699 plebiscyt, Archived at Wayback

700 Li R., Pei S., Chen B., Song Y., Zhang T., Yang W., Shaman J., 2020, Substantial undocumented infection facilitates
701 the rapid dissemination of novel coronavirus (SARS-CoV-2), *Science*, 368, 489

702 Lloyd-Smith J. O., Schreiber S. J., Kopp P. E., Getz W. M., 2005, Superspreading and the effect of individual
703 variation on disease emergence, *Nature*, 438, 355

704 Marsaglia G., Tsang W. W., Wang J., 2003, Evaluating kolmogorov's distribution, *J.Stat.Soft.*, 8, 1

705 Mebane W. R. J., 2010, Fraud in the 2009 presidential election in iran?, *Chance*, 23, 6

706 Millman K. J., Aivazis M., 2011, Python for scientists and engineers, *CiSE*, 13, 9

707 Molina-Cuevas E. A., 2020, Choosing a growth curve to model the Covid-19 outbreak, *arXiv e-prints* ,
708 (arXiv:2007.03779)

709 Munck G. L., Verkuilen J., 2002, Conceptualizing and Measuring Democracy: Evaluating Alternative Indices,
710 *Comparat.Polit.Stud.*, 35, 5

711 Newcomb S., 1881, Note on the Frequency of Use of the Different Digits in Natural Numbers, *American Journal of*
712 *Mathematics* , 4, 39

713 Nigrini M., Miller S. J., 2009, Data diagnostics using second order tests of Benford's Law,
714 *Auditing: J. Pract. & Theory*, 28, 305

715 Oliphant T. E., 2007, Python for scientific computing, *CiSE*, 9, 10

716 Papoulis A., Pillai U., 2002, Probability, Random Variables and Stochastic Processes, 4th edn. McGraw-Hill Europe

717 Poisson S.-D., 1837, Recherches sur la probabilité des jugements en matière criminelle et en matière civile ;
718 précédées des Règles générales du calcul des probabilités. Bachelier, Imprimeur-Libraire, Paris, [https://](https://gallica.bnf.fr/ark:/12148/bpt6k110193z/f218.image)
719 gallica.bnf.fr/ark:/12148/bpt6k110193z/f218.image

720 Porecha M., 2020, India records over 10,000 new Covid-19 cases for first time, *The Hindu* , [https://www.](https://www.thehindubusinessline.com/news/national/india-records-over-10000-new-covid-19-cases-for-first-time/article31810421.ece)
721 [thehindubusinessline.com/news/national/india-records-over-10000-new-covid-](https://www.thehindubusinessline.com/news/national/india-records-over-10000-new-covid-19-cases-for-first-time/article31810421.ece)
722 [19-cases-for-first-time/article31810421.ece](https://www.thehindubusinessline.com/news/national/india-records-over-10000-new-covid-19-cases-for-first-time/article31810421.ece), Archived at Archive Today

723 Reporters sans frontières 2021, Detailed methodology, <https://rsf.org/en/detailed-methodology>,
724 Archived at Archive Today

725 Robertson M. P., Hinde R. L., Lavee J., 2019, Analysis of official deceased organ donation data casts doubt on the
726 credibility of China's organ transplant reform, *BMC Medical Ethics*, 20, 79

727 Rouabah M. T., Tounsi A., Belaloui N. E., 2020, A mathematical epidemic model using genetic fitting algo-
728 rithm with cross-validation and application to early dynamics of COVID-19 in Algeria, *arXiv pre-prints* ,
729 (arXiv:2005.13516)

730 Roukema B. F., 2014, A first-digit anomaly in the 2009 iranian presidential election, *Journal of Applied Statistics*,
731 41, 164 (arXiv:0906.2789v6)

732 Roukema B. F., 2015, in Miller S. J., ed., , The Theory and Applications of Benford's Law. Princeton University
733 Press, Princeton, pp 223–232

734 Ruijter E., Détienné F., Baker M., Groff J., Meijer A. J., 2019, The Politics of Open Government Data: Understanding
735 Organizational Responses to Pressure for More Transparency, *Am.Rev.Publ.Admin.*, 50, 260

736 Schwarz G. E., 1978, Estimating the dimension of a model, *Ann.Statist.*, 6, 461

737 Sen P. K., 1968, Estimates of the regression coefficient based on Kendall's tau, *J. Amer. Stat. Assoc.*, 63, 1379

738 Shapiro S. S., Wilk M. B., 1965, An analysis of variance test for normality (complete samples), *Biometrika*, 52, 591

739 Smirnov N., 1948, Table for Estimating the Goodness of Fit of Empirical Distributions, *Ann. Math. Stat.* , 19, 279

740 Theil H., 1950, A rank-invariant method of linear and polynomial regression analysis, *Nederl. Akad. Wetensch.*,
741 *Proc.* , 53, 386

742 Thomas P., Lau M. K., Trisovic A., Boose E. R., Couturier B., Crosas M., Ellison A. M., Gibson V., Jones C. R.,
743 Seltzer M., 2017, If these data could talk, *Scientific Data*, 4, 170114

744 Wyrzykowski M., 2020, Former CT judge Prof. Wyrzykowski: The presidential elections in Poland will be held
745 under the pretence of legality, *Ruleoflaw.pl* , [https://ruleoflaw.pl/former-ct-judge-prof-](https://ruleoflaw.pl/former-ct-judge-prof-wyrzykowski-the-presidential-elections-in-poland-will-be-held-under-the-pretence-of-legality)
746 [wyrzykowski-the-presidential-elections-in-poland-will-be-held-under-the-](https://ruleoflaw.pl/former-ct-judge-prof-wyrzykowski-the-presidential-elections-in-poland-will-be-held-under-the-pretence-of-legality)
747 [pretence-of-legality](https://ruleoflaw.pl/former-ct-judge-prof-wyrzykowski-the-presidential-elections-in-poland-will-be-held-under-the-pretence-of-legality), Archived at Wayback

748 Yang L., Dai J., Zhao J., Wang Y., Deng P., Wang J., 2020, Estimation of incubation period and serial interval of
749 COVID-19: analysis of 178 cases and 131 transmission chains in Hubei province, China, *Epidemiol.Infect.*, 148,
750 e117

751 Yu H., Robinson D. G., 2012, The New Ambiguity of "Open Government", *UCLA L. Rev. Disc.*, 59, 178

752 van der Walt S., Colbert S. C., Varoquaux G., 2011, The NumPy Array: A Structure for Efficient Numerical Com-
753 putation, *CiSE*, 13, 22 (arXiv:1102.1523)

754 A JHU CSSE DATA

755 The John Hopkins University Center for Systems Science and Engineering global time se-
756 ries data was downloaded on 6 May 2021 from <https://raw.githubusercontent.com>.

Table A1. As in Table 1, for the JHU CSSE data: clustering parameters for the countries with the 10 lowest ϕ_i and 10 lowest ψ_i values, i.e., the least noise; extended version of table: zenodo.5261231/phi_N_full_jhu.dat.

country	ϕ_i' model					alternative analyses			
	N_i	P_i^{Poiss}	P_i^{KS}	ϕ_i	ψ_i	\hat{v}_i	ω_i	P_i^{KS}	ω_i
Syria	23121	0.48	0.94	0.72	0.004	0.94	0.72	0.48	0.00
Algeria	123272	0.04	0.19	0.98	0.002	0.20	1.00	0.04	0.00
Croatia	339412	0.27	0.89	3.24	0.005	0.89	3.24	0.70	1.02
Saudi Arabia	422316	0.00	0.83	3.67	0.005	0.66	3.55	0.62	2.43
New Zealand	2637	0.10	0.88	3.85	0.074	0.89	4.68	0.90	3.63
Albania	131419	0.00	0.16	4.90	0.013	0.17	4.90	0.09	3.76
Thailand	74921	0.29	0.99	5.37	0.019	0.99	5.37	0.96	3.80
Denmark	257182	0.00	0.97	5.56	0.010	0.99	5.56	0.91	5.50
Iceland	6498	0.33	1.00	5.96	0.073	0.99	5.96	0.95	4.27
Greece	352027	0.03	0.98	6.53	0.011	0.92	5.43	0.67	5.50
Algeria	123272	0.04	0.19	0.98	0.002	0.20	1.00	0.04	0.00
Russia	4792354	0.00	0.31	10.12	0.004	0.26	9.44	0.26	8.81
Syria	23121	0.48	0.94	0.72	0.004	0.94	0.72	0.48	0.00
Croatia	339412	0.27	0.89	3.24	0.005	0.89	3.24	0.70	1.02
Saudi Arabia	422316	0.00	0.83	3.67	0.005	0.66	3.55	0.62	2.43
Iran	2591609	0.00	0.33	11.61	0.007	0.17	10.00	0.25	9.66
Turkey	4955594	0.00	0.02	19.95	0.008	0.01	19.27	0.01	16.98
Denmark	257182	0.00	0.97	5.56	0.010	0.99	5.56	0.91	5.50
Hungary	785967	0.02	0.99	9.23	0.010	0.98	14.29	0.91	7.00
Belarus	363732	0.00	0.01	6.92	0.011	0.01	6.46	0.01	5.13

757 com/CSSEGISandData/COVID-19/master/csse_covid_19_data/
758 csse_covid_19_time_series/time_series_covid19_confirmed_global.csv,
759 from git commit 51CB3EE, and analysed using the same software and parameters as for the C19CCTF
760 data. Tables A1–A4 show the equivalent of Tables 1–4, respectively. The rankings and ϕ_i estimates
761 appear mostly similar between the two datasets, with small differences. One difference is that the low
762 ϕ_i^7 value for India shown in Table 4 is absent in Table A4. In other words, while the media stated that
763 the daily confirmed count in India first went above the 10,000-per-day psychological threshold on 12
764 June 2020 (Porecha, 2020), the JHU CSSE data crossed this threshold earlier, and contains noise that
765 was unknown at that time to the national Indian media and is absent from the C19CCTF data.

766 Another difference is that Saudi Arabia, Iran, and the United Arab Emirates have lowest-noise sub-
767 sequence dates detected in 2021 in the JHU CSSE Tables A2–A4, while no country has lowest-noise
768 subsequences in 2021 in the C19CCTF data (Tables 2–4). The relative strengths of the AIC and BIC
769 evidence in Table A5 are similar to those in Table 5, even though the values change.

770 Table A6 shows that the JHU CSSE data generally find somewhat stronger anticorrelations between
771 the clustering parameters and PFI^{2020} compared to Table 6.

Table A2. As in Table 2, for the JHU CSSE data: least noisy 28-day sequences – clustering parameters for the countries with the 10 lowest ϕ_i^{28} values; extended table: zenodo.5261231/phi_N_28days_jhu.dat.

country	N_i	$\langle n_i^{28} \rangle$	P_i^{Poiss}	P_i^{KS}	ϕ_i^{28}	starting date
Algeria	123272	338.2	0.02	0.72	0.05	2020-08-18
Turkey	4955594	1014.5	0.03	1.00	0.14	2020-06-30
United Arab Emirates	529220	2884.9	0.01	0.07	0.15	2020-12-30
Belarus	363732	921.9	0.14	0.89	0.21	2020-05-08
Albania	131419	203.8	0.33	0.64	0.23	2020-09-27
Russia	4792354	5414.0	0.36	0.85	0.24	2020-07-19
Saudi Arabia	422316	332.5	0.54	0.78	0.43	2021-02-01
Syria	23121	70.0	0.19	0.91	0.50	2020-08-15
Iran	2591609	6594.5	0.14	0.41	1.51	2021-01-15
Georgia	315913	384.4	0.79	0.99	1.66	2020-09-17

Table A3. As in Table 3, for the JHU CSSE data: least noisy 14-day sequences – clustering parameters for the countries with the 10 lowest ϕ_i^{14} values; extended version of table: zenodo.5261231/phi_N_14days_jhu.dat.

country	N_i	$\langle n_i^{14} \rangle$	P_i^{Poiss}	P_i^{KS}	ϕ_i^{14}	starting date
United Arab Emirates	529220	3384.1	0.07	0.35	0.05	2021-01-11
Algeria	123272	336.4	0.06	0.80	0.05	2020-08-26
Turkey	4955594	971.6	0.12	0.86	0.11	2020-07-08
Belarus	363732	945.6	0.22	1.00	0.13	2020-05-12
Albania	131419	143.4	0.16	0.92	0.15	2020-09-01
Saudi Arabia	422316	337.7	0.32	0.79	0.20	2021-02-08
Russia	4792354	5165.5	0.47	0.51	0.28	2020-08-01
Syria	23121	76.6	0.42	0.96	0.35	2020-08-14
Poland	2811951	299.9	0.55	0.68	0.53	2020-06-17
Kenya	161393	126.2	0.54	0.91	0.57	2020-06-03

Table A4. As for Table 4, for the JHU CSSE data: least noisy 7-day sequences – clustering parameters for the countries with the 10 lowest ϕ_i^7 values; extended table: zenodo.5261231/phi_N_07days_jhu.dat.

country	N_i	$\langle n_i^7 \rangle$	P_i^{Poiss}	P_i^{KS}	ϕ_i^7	starting date
United Arab Emirates	529220	544.9	0.24	0.99	0.05	2020-04-27
Turkey	4955594	929.6	0.22	0.93	0.05	2020-07-15
Albania	131419	297.7	0.23	0.98	0.05	2020-10-18
Belarus	363732	947.9	0.60	0.94	0.05	2020-05-13
Algeria	123272	204.3	0.37	0.49	0.05	2020-10-14
Russia	4792354	5035.0	0.38	0.75	0.10	2020-08-09
Poland	2811951	297.0	0.51	0.99	0.10	2020-06-20
Saudi Arabia	422316	175.6	0.52	0.99	0.15	2021-01-13
Syria	23121	82.3	0.21	0.97	0.17	2020-08-14
Panama	365975	171.1	0.82	0.96	0.17	2020-05-09

Table A5. As for Table 5, Akaike (1974) and Bayesian (Schwarz, 1978) information criteria for the ϕ_i' and alternative analyses for the JHU CSSE data; plain-text version: zenodo.5261231/AIC.BIC_full_jhu.dat.

model	ϕ_i'		log. median		neg. binomial		2-day grouping		3-day grouping	
	AIC	BIC	AIC	BIC	AIC	BIC	AIC	BIC	AIC	BIC
	376.18	994.94	401.69	1020.44	498.00	1116.75	421.96	1032.94	239.83	811.89

Table A6. As for Table 6, Kendall τ statistic and its significance (two-sided) P^τ for the null hypothesis of no correlation between the ranking of PFI²⁰²⁰ and ϕ_i or ψ_i for the full data or subsequences, for the JHU CSSE data; plain-text version: zenodo.5261231/pfi_correlations_table_jhu.dat.

parameter	full		28-day		14-day		7-day	
	τ	P^τ	τ	P^τ	τ	P^τ	τ	P^τ
ϕ_i	-0.124	0.105	-0.158	0.0400	-0.175	0.0230	-0.232	0.00254
ψ_i	-0.165	0.0318	-0.162	0.0346	-0.163	0.0339	-0.194	0.0112